Abstract

The assembly of the branched actin network generates the force required for cellular functions such as cell motility and endocytosis. During assembly, the network experiences resistance from the membrane and can adapt to the resistive force by modulating its own growth speed, branch density, and architecture both *in vivo* and *in vitro*. After assembling, the network must be rapidly disassembled so it can be used elsewhere. Similar to while assembling, the network experiences force while disassembling. However, how forces affect the disassembly of the network is unknown, specifically dissociation of Arp2/3 complex branches. I applied a wide range of pulling forces to Arp2/3 complex branches using microfluidics and used fluorescence microscopy to measure the lifetime of the branches as a function of force. I found that small pN forces can accelerate debranching more than 200-fold, from hours to <1 min. The Arp2/3 complex can exist in two unique mechanical states which I termed "young/strong" and "old/weak" because "old/weak" branches are more sensitive to force and dissociate faster under force than the "young/strong" branches under force. Branches transition from "young/strong" to "old/weak" over time and the transition is triggered by phosphate release. Lastly, the debranching protein Glia Maturation Factor (GMF) specifically targets "old/weak" branches over "young/strong" for dissociation. Taken together, these findings suggest that force and GMF could preferentially disassemble older portions of the network by targeting "old/weak" Arp2/3 complexes that have released phosphate.

Mechanical Properties Of The Arp2/3 Complex

A Dissertation
Presented to the Faculty of the Graduate School
Of
Yale University
In Candidacy for the Degree of
Doctor of Philosophy

By
Nandan Gajanan Pandit

Dissertation Directions: Enrique M. De La Cruz

May 2020

Contents

Acknowledgements

I first thank my parents Gajanan M. Pandit (father) and Vandana G. Pandit (mother) for migrating from India to the United States in search for a better life and in pursuit of the American dream. Moving to the U.S. with little financial, social, or familial support was filled with numerous stressful challenges and hurdles. So, I thank you for enduring this journey, and intrepidly providing a prosperous life for Rohan (brother) and I. Thank you for caring for us and nurturing us every moment since birth. Thank you for continuously and reliably providing a safe environment for us to grow, learn, and develop. From you I learned right from wrong, generosity, and how to be a good member of the community. We will continue to grow your legacy through our own hard work for the people around us. Dad, please go to the doctor once in while. Mom, please exercise more.

I would like to thank my brother Rohan for always being a reliable friend and partner. Growing up with him has provided me with numerous and invaluable joys such as playing made-up games in our basement, riding bikes, playing video games, swimming at the pool, and talking about our lives and goals. It has been an immense pleasure having someone to talk to about shared experiences and seeing you grow into a respectable and caring individual. I learned generosity from you and I will learn much more over the years.

I would like to thank Dr. Mike Lemieux, Dr. Jordan Greco, and Dr. Nicole Wagner, and Dr. Robert Birge for seeding and nurturing my interest in research. I learned that research was a viable career path from Dr. Lemieux and his suggestion to join a research lab changed the trajectory of my life. I worked very closely with Dr. Wagner and Dr. Greco as an undergraduate research assistant and learned a great deal about molecular biology and designing new assays from them. Perhaps more importantly, I

learned how to be a good colleague and scientific community member. Finally, I would like to thank Dr. Birge for allowing me to work in his laboratory and showing me how fun science can be. I fondly remember attending his classes and spending a significant section laughing and the rest of the time learning about programming and chemistry.

I would like to thank Robert Stickels for his reliable friendship for almost a decade. Bob and I met as sophomores at UCONN and we continuously supported each other as we worked hard in our research labs and for coursework. His reliable attitude towards work and friendship has been invaluable to me, especially as I looked to him for motivation in college. I hope that we continue to be best friends through life and continue to support each other in the pursuit of our dreams.

I would like to thank the wonderful community of friends and colleagues at Yale that I met through classes, MBB activities, and at the graduate bar Gypsy. Their friendships have been critical to succeed in graduate school because I could always count on their support in times of need. From first year, where we all needed to rely on each other for help in classes to the final defense presentation, where we helped each other with prepare the talks. In addition to the science, I am grateful for the numerous activities we did together like hiking, trips, and countless pot-lucks. I will remember the time spent with them with immense joy and hope to continue to see them in future years.

I would like to thank Wei Ng for her generous support in the last 2 years of graduate school, help in reading my dissertation, and her feedback on my defense. Her help was critical to improve the quality of the work and many of her questions were as challenging as the reviewers. I am grateful for her continuous support as I transition into

my career and I feel lucky to have such a reliable friend and partner as I move forward through life.

I would like to thank the Pathways to Science Community at Yale, especially Maria Parente for allowing me to teach in Pathways. It has been a tremendous opportunity to design a course with Dr. Luke Burkhart and Danny Seara and teach young students how to code and run computer simulations. I will remember these memories fondly and hope to continue working with Pathways and similar programs in the future.

I would like to thank the lab members of the De La Cruz lab for contributing to and maintaining an excellent place to work. Each student has their own project/research but is eager to help each other. For that reason, projects are high quality because they draw upon everyone's expertise. I will surely miss our 2pm coffee time where we talked about science and life. Specifically, I would like to thank Dr. Anthony Schramm, Dr. Jeff Bibeau, and Shawn Gray for their near daily feedback and suggestions. Working with them has made my thesis work specifically much more productive. I encourage future students to continue developing such relationships as they are both critical for scientific productivity and happiness.

I would like to thank Dr. Wenxiang Cao for his tremendous help with my thesis work as well his help writing the paper. Having an experienced and helpful research scientist in the lab has been an invaluable experience. I believe I asked Wenxiang a question everyday of my PhD and I cannot remember even one time he did not spend time to help me. So, I have learned so much from him. Additionally, his happy and jocular attitude has helped all students in the lab when projects were not working and he has shared in the joys of other's projects when they succeeded. His contribution to my

and other students has been extremely important and I hope he continues to mentor and help students in the future.

I would like to thank my committee Dr. Charles Sindelar, Dr. Mark Hochstrasser, and Dr. Thomas Pollard for their guidance over the last few years. My initial project (Chapter 3) did not produce the expected results and so it was challenging to publish. My committee supported me while I found other projects to work on. After performing the initial experiments for Chapter 2 my committee was extremely supportive and encouraged me to switch projects which I believe was important to completing my Ph. D. I would like to specifically thank Dr. Thomas Pollard for his help with writing the manuscript. Through his guidance we wrote a much more concise and clear manuscript which will allow the work to really be well understood and appreciated.

Last, but surely not least, I would like to thank my advisor, teacher, and mentor Dr. Enrique M. De La Cruz. I learned a great deal of both science and life from Enrique. First, I would like to thank Enrique for creating and actively maintain an environment where students can grow and develop into independent scientists. Enrique prioritizes the well-being of his trainees and this attitude creates deep and long-lasting bonds between Enrique and his trainees. There is no doubt that Enrique teaches the trainees in the lab about science, writing, thinking about projects etc, but perhaps more importantly he teaches trainees how to be contributing members of the scientific community. Lastly, I would like to thank Enrique for being a consistent positive role model for students to look up. Thank you for your tireless efforts and I hope future trainees get to benefit from your efforts as well.

Chapter 1 – Introduction

In the introduction of this dissertation I provide an overview of the actin cytoskeleton and key information required to understand the work presented here. I begin with a basic introduction to the main components of the branched actin network and its function. I discuss the structural properties of the branched actin network and the role of the structural properties in the function of the network. I introduce how the branched actin network is regulated and turned over in addition to the critical role of the nucleotide bound to actin and Arp2/3 complex. Last, I discuss how forces can affect branched actin network assembly and disassembly.

1.1 Main components and assembly of the branched actin network

The main components of the branched actin network are actin, the Arp2/3 complex, and cross-linking proteins such as fimbrin. The focus of my dissertation is on the mechanical properties of the Arp2/3 complex. So, below I discuss details on the structure, function, and regulation of actin filaments and Arp2/3 complex.

Actin

Actin is a highly conserved 42 kD globular protein and with a critical role in many cellular functions such as cell motility, endocytosis, trafficking (1). Globular actin, known as G-Actin, can polymerize into filaments called F-Actin. F-actin filaments have two distinct ends called the barbed end (also known as the plus end) and pointed end (also known as minus end) and the ends grow at different rates. The polymerization, biochemical properties, and structure of actin filaments has been well studied with

reconstituted systems *in vitro* and provides valuable knowledge that is required to understand the complex function of actin networks within the cell (2).

Hydrolysis & and phosphate release from actin

Actin is an ATPase and the ATPase cycle allows for a broad range of biochemical, and consequently biophysical, regulation. Actin hydrolyzes ATP as it polymerizes into filaments (3). Perhaps more important than the rate of hydrolysis is the rate of phosphate release since it is the rate limiting step in the ATPase cycle of F-Actin, excluding depolymerization and release of ADP from monomeric actin (4). Phosphate release is linked to many biochemical properties such as assembly/disassembly rates and regulation by proteins such as cofilin (5). Since phosphate release is often coupled with large conformational changes (6), it is reasonable to expect that phosphate release is coupled with a large structural change in F-Actin. However, a recent cryo-EM structure of actin bound to different nucleotides (AMPPNP, ADP-Pi, and ADP) revealed that the structure is surprisingly similar (7). The authors conclude that structural changes in the actin are primarily controlled by the assembly of actin (i.e. actin flattens when polymerized from G-Actin to F-Actin) and not the nucleotide. Phosphate release can control the affinity for actin regulatory proteins such as cofilin, discussed in the following section (5). To summarize, the ATPase cycle of actin and particularly the phosphate release plays a large role in the regulation of actin filaments and in this work, I show that phosphate release from the Arp2/3 complex plays a similarly important role.

Arp2/3 complex

Actin related protein (Arp2), actin related protein (Arp3), and 5 other protein subunits comprise the Arp2/3 complex and together with actin, forms the branched actin network

(1). The Arp2/3 complex binds to the side of preformed actin filaments, must be specifically activated by membrane bound proteins, and then initiates the formation of a "daughter branch" (8). The interface between the Arp2 and Arp3 proteins and actin comprise the majority of the interface between the Arp2/3 complex the daughter filament and the remaining subunits primarily interact with the mother filament (9). The assembly of the branched actin network generates the force required for essential functions like cell motility and endocytosis (10). The branched actin network can be clearly seen in the lamellipodia of cells via electron microscopy (11, 12). With purified minimal protein components, the branched actin network can also be reconstituted *in vitro* indicating that scientists have identified the minimal components of the network and have at least a basic idea of how the network functions and its role in motility (13, 14).

Arp2/3 complex activation

The Arp2/3 complex must be activated before branch initiation and both branch initiation and debranching are tightly linked with the nucleotide state of the Arp2/3 complex (15-17). Similar to actin, the Arp2/3 complex is an ATPase and it must bind to ATP to form branches (17). In cells, the Arp2/3 complex activation primarily at the cell membrane by membrane bound activators such as WASP (12). In vitro, the Arp2/3 complex can be activated by the minimal portion of the activator the called VCA (Verprolin Central Acidic) domain (18, 19). The common feature in these activators and methods is that the Arp2/3 complex nucleates new branches off the mother filament. Recently, another group discovered a new class of activators that can activate Arp2/3 complex without mother filaments (20) and this class of activators was characterized in detail by the Nolen Lan (21).

The role of the ATPase cycle of the Arp2/3 complex

The role of the ATPase cycle of the Arp2/3 complex remains unclear because there are inconsistent reports but most evidence suggests that ATP is required for branch formation and phosphate release usually precedes debranching (15, 17, 22, 23). Using reconstituted proteins, the Carlier lab reported that hydrolysis is slow (half-life ~800 seconds) and hydrolysis triggers debranching. Additionally, this study suggested that only hydrolysis from the Arp2 subunit of the Arp2/3 complex was relevant, not the Arp3 subunit. In contrast, the Mullins lab reported that hydrolysis occurs almost immediately after branch formation and phosphate release occurs shortly after (<1 min). They do not comment on how hydrolysis affects debranching. Since branches can have long lifetimes, >~60 min, this indirectly implies that phosphate release (occurs in less than ~40 min) does not trigger debranching which is in direct contrast to the Carlier lab. The Drubin lab made mutations in the Arp2/3 complex to reduce the rate of hydrolysis and observed that branches formed with mutant Arp2/3 complex have longer lifetimes than WT Arp2/3. Interestingly, mutations into both Arp2 and Arp3 subunits that abrogate hydrolysis decrease hydrolysis and consequently reduce the rate of debranching. This is at odds with the Carlier lab because they report only the Arp2 subunit is important for hydrolysis and subsequently triggering debranching. They conclude that ATP hydrolysis accelerates debranching but their data could not distinguish whether hydrolysis or phosphate release is the relevant reaction. In Chapter 2, I present data and an interpretation that favors phosphate release controlling debranching rather than hydrolysis, consistent with the Mullins lab. Since each group used different assays and different sources of the Arp2/3

complex, it is challenging to identify with certainty the role of ATP hydrolysis in the Arp2/3 complex and so the role of the ATP cycle will require more investigation.

1.2 Structural properties of the branched actin network

To gain mechanistic insight into how the branched actin network generates and sustains force, it is important to understand each component of the branched actin network (actin, Arp2/3 complex, and cross-linkers) and how each component influences one another. In Chapter 3 of this dissertation, I investigate the mechanical properties of the Arp2/3 complex branches and so provide a brief introduction with relevant information. Briefly, my goal was to understand if site specific cation could control the branch angle and mechanical properties of the Arp2/3 complex.

Mechanical properties of the Arp 2/3 complex

The molecular origins (e.g. the specific amino acids, binding interfaces, salt binding sites, or protein-protein interactions) of the Arp2/3 complex branch junction stiffness are unknown. The Arp2/3 complex characteristically forms branches at ~70° degrees ± ~10° as observed both *in vitro* and *in vivo* but the molecular origins for this particular angle is unknown (8, 11, 24) . Both mean and variation of the branch angle can vary depending on the Arp2/3 complex isoform (25), however the mean angle is usually between ~70° and ~80°. The most likely explanation is because the angle orients the growing daughter filament to favorably generate force against the membrane (26). Some theoretical studies suggest that other branch angles may be less favorable for force generation (27). So, maintaining the stiffness of the Arp2/3 complex branch angle is probably important to effectively generate force. Blanchoin *et al* reports a rotational spring constant of the

Arp2/3 complex branch angle and I use a similar metric in Chapter 3 of this dissertation to measure branch angle stiffness (25).

Based on how cations can modulate the stiffness of actin filaments, the De La Cruz lab hypothesized that perhaps cation binding at the interface between the Arp2/3 complex and the daughter filament provides structural rigidity and could control the ~~70° degrees branch angle (28). I tested this hypothesis in Chapter 3 of this dissertation. The data was inconclusive but there was no observable effect of cations on the branch angle stiffness/rigidity in most of the experiments I present.

1.3 Regulation of protein components

Network turnover

One of the leading hypotheses that describes the structure and function of the branched actin network is the dendritic nucleation hypothesis and it is supported by a large body of evidence (2). In the dendritic nucleation hypothesis, actin polymerization is concentrated at the edge of the membrane in the growing barbed ends of the branched actin network. Consequently, the growing ends push older portions of the networks backwards away from the membrane. As the network ages and is no longer needed to generate force, it is disassembled and the actin monomers and Arp2/3 complexes are recycled to be reassembled at the leading edge of the cell. A complex regulatory mechanism is required to maintain precise turnover of this network.

Nucleotide and aging

One method of regulating network turnover is by favoring older portions of the network for disassembly by identifying and targeting its nucleotide state. ATP hydrolysis acts as a

timer/indicator for the age of the network. Newly formed portions of the network are mostly in ADP-P_i state, due to the fast hydrolysis of ATP and slow phosphate release (4). Older portions of the network are bound primarily to ADP because over time they hydrolyzed the bound ATP and released phosphate (12). Regulatory proteins such as cofilin target ADP actin for binding and severing and this targeting provides one mechanism to target older portions of the network for disassembly (5). My dissertation has shown that other regulatory proteins such as Glia maturation factor (GMF) (29), a protein similar to cofilin, can also target older Arp2/3 complex branches for debranching similar to cofilin severing older filaments. My contribution that GMF targets older branches for debranching is consistent with the current dendritic nucleation hypothesis and provides more one component (cofilin targets older ADP actin filaments) for regulation related to the nucleotide state of the branched actin network.

1.4 Forces on branched actin networks

How forces affect the assembly of branched actin networks

Branched actin networks can adapt to forces both *in vivo* and *in vitro* by controlling parameters such as growth speed, density, and architecture. The Mullins and Fletcher labs showed that networks adapt to compressive forces applied by AFM by increasing the density of branches within the branched actin network and consequently power (30). Adapting to the forces can also provide the networks with a "memory" and can be explained in the following way. As the network grows, a temporary increase in force can result in a temporary increase in branch density. This could be due to increased branching on concave bent filaments (31). When the force is released, the branching rate returns to normal but the branches that were generated during the time of applied force are still

present in the network but are pushed backwards as the leading edge of the network grows. A strikingly similar pattern of memory was also seen in cells (32). The authors applied force to the cell membrane with suction from a micro pipettor and observed that the network within the cell adapted by increasing density. After the force was released, the portion of the network with higher branch density could be seen traveling backwards away from the membrane as the network turned over. Authors also noted that the architecture of the network was altered with applied load.

How forces could affect disassembly of branched actin networks

Forces may also be able to affect the disassembly of branched actin networks and this is the major focus of my dissertation. Since force regulates the assembly of branched actin filaments, I asked the question if debranching could be affected by force. Originally, I was most interested in understanding if cofilin dependent debranching could be affected by force because cofilin severing was thought to be reduced by tension on actin filaments (33). I hypothesized that cofilin debranching activity could be dampened by force. Before testing this hypothesis, I first completed the control to determine if force might influence the dissociation of branches formed by the Arp2/3 complex and found that it does (Chapter 2). Along the way I found an interesting mechanism by which the Arp2/3 complex can regulate its own sensitivity to force. Immediately after branch formation the (within less than 40s), Arp2/3 complex is bound to ADP-P_i (15). After the Arp2/3 complex releases the phosphate, the Arp2/3 complex shifts into a weak state and is very sensitive to debranching by force compared to the strong state ADP-P_i which is far less sensitive to force. The nucleotide state of the Arp2/3 complex also controls the ability of

GMF to dissociate branches. Future studies might study if regulatory proteins such as GMF and cortactin may also affect the sensitivity to force.

Chapter 2 – Force and phosphate release from the Arp2/3 complex promotes debranching

This chapter was taken from a manuscript which is in revision at PNAS as "Force and phosphate release from Arp2/3 complex promote dissociation of actin filament branches".

This work and resulting manuscript was a collective effort, and in this paragraph I describe who completed each which portion of the project to the best of my memory and records. I conceived the first iteration of the project and with extensive advice, support, and guidance from Professor Enrique M. De La Cruz the project design was greatly improved throughout the process. Dr. Eric Johnson constructed the microfluidics device and showed me how to use his set-up on the TIRF microscope. I optimized the microfluidics assay (surface functionalization) and developed the novel assays used in this chapter. I performed all experiments and generated all required reagents (DNA constructs, purified proteins, etc.). Dr. Jeffrey Bibeau performed single molecular tracking of the labeled Arp2/3 in Fig. 1D and 1C and he created Fig. 1C and 1D. Dr. Wenxiang Cao constructed the mathematical model and used his model to analyze some of the time courses and fit rate constants to the data, particularly Fig 3B and Fig 10C. Dr. Wenxiang Cao made Fig 2A/B, 10B and Fig 11. In the text, some of these equations refer to a derivation in the *SI Appendix* which was written entirely by Dr. Wenxiang Cao with editing from all authors. So, I refer to the SI Appendix which is in revision in the above

paper, but do not include it in this dissertation because it is not my original work. I performed the first iteration of analysis for all experiments and then received critical guidance from all authors to improve the analysis, especially Dr. Wenxiang Cao who helped fit fitting some data and formatting plots. I wrote the first draft of the manuscript which was followed by significant editing by all authors on the manuscript, specifically Dr. Wenxiang Cao, Professor Enrique M. De La Cruz, and Professor Thomas D. Pollard. I would like to specifically thank Professor Thomas D. Pollard for his extensive editing which significantly improved the presentation of data and readability of this manuscript.

2.1 Abstract

Networks of branched actin filaments formed by Arp2/3 complex generate and experience mechanical forces during essential cellular functions including cell motility and endocytosis. External forces regulate the assembly and architecture of branched actin networks both *in vitro* and in cells. Considerably less is known about how mechanical forces influence the disassembly of actin filament networks, specifically the dissociation of branches. I used microfluidics to apply force to branches formed from purified muscle actin and fission yeast Arp2/3 complex and observed debranching events in real time with TIRF microscopy. Low forces in the range of 0-2 pN on branches accelerated their dissociation from mother filaments more than two orders of magnitude, from hours to <1 min. Neither force on the mother filament nor thermal fluctuations in mother filament shape influenced debranching. Arp2/3 complex at branch junctions adopts two distinct mechanical states with different sensitivities to force, which I name "young/strong" and "old/weak". The "young/strong" state 1 has ADP-P_i bound to Arp2/3 complex. Phosphate release converts Arp2/3 complex into the "old/weak" state 2 with bound ADP, which is 20 times more sensitive to force than state 1. Branches with ADP-Arp2/3 complex are more sensitive to debranching by fission yeast GMF (glia maturation factor) than branches with ADP-P_i Arp2/3 complex. These findings suggest that aging of branch junctions by phosphate release from Arp2/3 complex and mechanical forces contribute to disassembling "old" actin filament branches in cells.

2.2 Introduction

Arp2/3 complex forms networks of branched actin filaments that generate and sustain mechanical forces that power cell motility, endocytosis, and vesicle trafficking (10, 34). Membrane bound proteins, called nucleation promoting factors, such as WASP activate Arp2/3 complex, which then nucleates a branch when it binds to the side of a pre-existing 'mother' filament (1). The new 'daughter' filament elongates and pushes against the membrane until it is capped. All of the filaments, including branches formed by Arp2/3 complex, must disassemble for recycling to form new filaments and branches. Similar to actin, Arp2/3 complex is an ATPase (17, 23, 24). Hydrolysis of bound ATP and subsequent phosphate release have been implicated in controlling branched network dynamics (15-17, 22, 35), but mechanistic details are lacking.

The assembly and architecture of branched actin networks are sensitive to force *in vitro* and in cells (36, 37). Under load, branched actin networks assembled from purified proteins grow more slowly and with a higher branch density (30, 38), but how these mechanical forces directly affect the biochemical interactions of branched actin network protein components has not been firmly established. Similar to measurements with purified protein components, branched actin networks in cells respond to external load by increasing density of branched filaments while also reorganizing relative to the membrane (32).

Networks of branched actin filaments turn over much more rapidly in cells than *in vitro* when assembled from purified proteins (39-42). The regulatory proteins cofilin and glia maturation factor (GMF) accelerate debranching and have been implicated in accelerating branched network remodeling and turnover (29, 43-46). Although not

investigated previously, mechanical forces may also affect network disassembly through debranching.

I report that mechanical forces promote dissociation of branches formed by Arp2/3 complex and that phosphate bound to Arp2/3 complex regulates the sensitivity to force. Phosphate release from Arp2/3 complex at branch junctions also regulates debranching by GMF. Thus, phosphate release from the Arp2/3 complex could target "older" ADP-Arp2/3 branches for dissociation while sparing "younger" branches with ADP-P_i Arp2/3 complex.

2.3 Results

Microfluidics assay to measure dissociation of branches formed by Arp2/3 complex under force.

I used fluid flowing through a microfluidics apparatus to apply force to actin filament branches formed by purified fission yeast Arp2/3 complex and muscle actin monomers (Fig. 1A) as I observed the dissociation of the branches by fluorescence microscopy. Starting with short filament seeds tethered to the surface of the slide, I assembled branched filaments from purified ATP-actin monomers and Arp2/3 complex for 2-4 min. After washing out the soluble proteins, the filaments were allowed to "age" for an additional, variable time with very slow fluid flow. Thereafter, I started the debranching process under constant force by flowing buffer over the surface at a rate of 2 – 500 μL min^{-1} until the end of the experiment, while I recorded a series of images. The seeds were immobilized on the slide, but both the mother filaments and branches were free to fluctuate (Fig. 1A).

Rapid flow rates flattened branches against the mother filaments until they dissociated (Fig. 1B, Movies S1-S3). Neither the angle of the applied force (relative to mother filament orientation), the tension in the mother filament, nor fluctuations in mother filament shape had a strong influence on debranching (Fig. 2C and D).

I added a snap tag to the Arpc5 subunit of Arp2/3 complex for labeling with Alexa-488 and simultaneous viewing with 647-Alexa labeled actin. Force dissociated Arp2/3 complex and the daughter filament concurrently, within the 0.1 s time resolution of the imaging (Fig. 1D; Movies S4-S5). Buffer flowed across the sample at 500 μm s^{-1} dissociated both the daughter filament and Arp2/3 complex from the field of view by the

next frame, making it impossible to determine if the labeled Arp2/3 complex remained bound to the dissociated daughter filament.

Piconewton forces decreased the time for branch dissociation from hours to <1 min. Branches formed by ATP-Arp2/3 complex were stable for many minutes without buffer flow (Fig. 3A) but had a higher probability of dissociating when subjected to the forces produced by the range of buffer flow rates in the experiments (Fig. 3A). The following sections explain how the time course of debranching depends on the applied force and how long the newly formed branches were aged after assembly. At a given flow rate the force on a branch scales with its length. In some experiments I show the force on individual branches (Fig. 4), but in most experiments I report flow rates from which I calculate the average force on branches (e.g. Fig. 3A).

In samples of branches formed by ATP-Arp2/3 complex and aged for 30 min, the time course of debranching followed a single exponential that depended on the applied force (Fig. 3A). The observed lifetimes of these branches decreased with force (Fig. 3D), suggesting a slip bond behavior, so I used the Bell's equation (47) (Eq. 1) to estimate the force sensitivity:

$$\tau_{obs} = \tau_0 e^{-\frac{Fd}{k_B T}} \quad (1)$$

Here k_B is the Boltzmann constant T is the absolute temperature, F is force, and τ_0 is the branch lifetime in the absence of force, d is the characteristic distance to the transition state (48). The value of d is typically considered a force sensitivity parameter for bond rupture. An alternative estimate of force-dependence is the force that reduces the

branch lifetime by half (half force, $F_{1/2} = 0.693 k_B T/d$), which I estimate to be 0.054 (± 0.008) pN.

Without force, the branch lifetime (τ_0), estimated from extrapolation of the fit of the force-dependence (Fig. 3D), was 106 (± 8) min (Table 1, $k_2 \sim 1/\tau_0 = 0.01$ (± 0.0007) min^{-1}), indicating that sustained pN forces reduce τ_{obs} more than two order of magnitude to <30 s. The force-dependence of individual branch lifetimes (Fig. 4) yielded a half force ($F_{1/2}$) of 0.054 (± 0.008) pN and $\tau_0 = 96$ (± 6) min, comparable to the values estimated from exponential fits of debranching time courses (Figs. 2A and D).

Branches assembled from ATP-Arp2/3 complex dissociate faster under force as they age.

As they age, branches assembled from ATP-Arp2/3 complex dissociated progressively faster under force produced by a buffer flow rate of 500 μL min^{-1} (Fig. 3B). Immediately after the 2.6 min assembly reaction, when the dominant nucleotide bound to both Arp2/3 complex and the actin filaments is expected to be ADP-P_i, the time course of branch dissociation followed a single exponential with a slow observed lifetime ($\tau_{s,F}$, where the subscript *F* indicates under flow force) of 3.08 (± 0.05) min corresponding to a first order rate constant $k_{s,F}$ of 0.32 (± 0.005) min^{-1}. Thus branches dissociated before a substantial fraction of the phosphate dissociated. After aging for 30 min, when both Arp2/3 complex and the subunits in the actin filaments are expected to have bound ADP, the time course of debranching also followed a single exponential with a 20-fold shorter lifetime ($\tau_{f,F}$) of 0.15 (± 0.01) min ($k_{f,F} = 6.67$ (± 0.44) min^{-1}**)**. At intermediate aging times, the time courses followed double exponentials (Fig. 3B) with distinguishable fast and slow phases, indicating that (at least) two reactions contributed to debranching.

To evaluate how force affects slow and fast debranching, we aged samples for a short time (~4 min), so the sample would include mixtures of branches with Arp2/3 complex with bound ADP-Pi and ADP and thus exhibit both slow and fast phases of dissociation over a range of forces applied with different flow rates. However, the actual ageing times prior to making observations varied. This uncertainty influenced the observed amplitudes but not the observed lifetimes, so we only analyzed the lifetimes. The debranching time courses at forces >1 pN followed double exponential decays (Fig. 2C), yielding the force dependence of the slow and fast phase lifetimes (Fig. 2D and inset; triangles). The lifetimes of the slow phase (2-4 min range) differed from the fast phase (0.3 – 0.8 min) in this force range (>1 pN) but neither depended strongly on the applied force. At low forces < 0.6 pN, dissociation of branches formed from ATP-Arp2/3 complex followed single exponentials, with lifetimes similar to branches with ADP-Arp2/3 complex (Fig. 2D). At forces less than < 0.6pN, the strong state branches in the ADP-Pi were present as well, but did not dissociate because of the low forces applied.

The debranching model presented below accounts for these different time courses. The fast phase lifetime behaved similar to ADP-Arp2/3 complex branches (i.e. assembled from ATP-Arp2/3 complex and aged 30 min), consistent with fast debrnching population corresponding to ADP-Arp2/3 complex branches. I discuss the force-dependence of the slow phase below.

The nucleotide bound to Arp2/3 complex influences the sensitivity of branches to force. ATP-Arp2/3 complex hydrolyzes the bound nucleotide upon or soon after branch formation (15, 17) followed by dissociation of the gamma-phosphate with an unknown rate constant. Therefore, branches formed by ATP-Arp2/3 complex rapidly transition to

the ADP-P_i state for an unknown duration before the release of P_i. Actin filament branches formed by Arp2/3 complex with mutations that slow ATP hydrolysis are more stable than those formed by native Arp2/3 complex, so Martin *et al.* proposed that the hydrolysis of ATP bound to Arp2/3 complex destabilizes branches (22).

I performed a series of experiments to determine if the nucleotide state of Arp2/3 complex could explain the slow and fast debranching states (Fig. 3B and 3C). Like *Acanthamoeba* Arp2/3 complex (17), *S. pombe* ADP-Arp2/3 complex did not form branches from ATP-actin monomers nor did the ADP-Arp2/3 complex form branches in the presence of 20 mM phosphate, (Fig. 5). A likely interpretation of this behavior is that the transient intermediate ADP-P_i-Arp2/3 complex is competent to form branches, but ADP-Arp2/3 complex binds P_i very weakly (K_d > 20 mM). On the other hand, *S. pombe* ADP-Arp2/3 complex formed branches with 2 mM beryllium fluoride (BeF_x) in the buffer (*SI Appendix*, Fig. 5), as originally shown for *Acanthamoeba* Arp2/3 complex (17). ATP-Arp2/3 complex also forms branches with 2 mM BeF_x in the buffer.

Branches with ADP-BeF_x Arp2/3 complex dissociate with indistinguishable time courses whether assembled from ATP-Arp2/3 complex or ADP-Arp2/3 complex in the presence of 2 mM beryllium fluoride and aged 4 min (Fig. 6). I assume that in both cases BeF_x binds to the ADP-Arp2/3 complex and stabilizes conformations similar to ADP-P_i, as established for actin (49, 50), so I used ADP-BeFx Arp2/3 complex branches made with either method. ADP-BeF_x-Arp2/3 complex branches aged for 4 or 30 min in the presence of 2 mM BeF_x dissociate with similar time courses and follow single exponentials (Fig. 3B). Thus, branches did not convert from the slowly to the rapidly dissociating state when aged with BeF_x.

Force is required to dissociate, within the experimental observation period, ADP-BeF_x-Arp2/3 complex branches formed from ATP-Arp2/3 complex in the presence of 2 mM BeF_x (Fig. 3C inset). Under low forces (i.e. <<0.6 pN), <20% of branches with ADP-BeF_x-Arp2/3 complex dissociated within 5 h, so branching lifetimes could not be measured reliably. With forces > 0.6 pN branches dissociated with single exponential time courses and observed rate constants (inverse of lifetimes) that depended on the applied force (Fig. 3C inset). Therefore, branches with ADP-BeF_x-Arp2/3 complex were more stable under force than branches with ADP-Arp2/3 complex (formed from ATP-Arp2/3 complex and aged for 30 min; Fig. 3D).

Under a given force, the lifetimes of ADP-BeF_x-Arp2/3 complex branches were longer (~2 fold) than the slow debranching phase of ATP-Arp2/3 complex branches that had been aged 4 min (Fig. 3D). The observed rate constant of the slow phase debranching reflects the *sum* of the ADP-P_i state debranching rate constant and the rate constant for conversion of the ADP-P_i-Arp2/3 complex to the ADP state (see *Discussion*).
It is therefore expected to be faster than ADP-BeF_x Arp2/3 complex debranching, which converts more slowly to ADP-Arp2/3 complex (Fig. 3B).

The nucleotide state of the actin filaments does not influence debranching.
I assembled branches from ATP-Arp2/3 complex with ADP or ADP-P_i bound to the subunits in the actin filaments and observed that all had similar time courses of debranching after aging for a given time (Fig. 7). Samples with ADP-actin filaments were prepared by assembly from ATP-actin monomers and ATP-actin Arp2/3 complex followed by aging for 30 min. Samples with ADP-P_i actin filaments were prepared by assembly from ATP-actin monomers and ATP-Arp2/3 complex in buffer containing 20

mM phosphate followed by aging for 4 or 30 min (Fig. 7). This concentration of phosphate is well above the K_d for binding ADP-actin subunits (51), so subunits in the filaments likely had ADP-P_i in the active site, assuming that Arp2/3 complex binding does not dramatically change the affinity of actin for phosphate. Samples assembled from ATP-actin monomers and ATP-Arp2/3 complex followed by 4 min aging had a mixture of ADP and ADP-P_i nucleotide states for both actin subunits and Arp2/3 complex. Samples with AMPPNP-actin (a non-hydrolyzable analog of ATP) were assembled from AMPPNP-actin monomers and ATP-actin Arp2/3 complex in buffer containing 2 mM AMPPNP followed by aging for 4 min. Since AMPPNP-Arp2/3 complex does not form branches ((17); Fig. 5), all of the branches formed from Arp2/3 complex with bound ATP, while the actin filaments had bound AMPPNP. A previous study of bovine Arp2/3 complex (39) reported more branches on mother filament segments with ADP-P_i than segments with ADP. This difference was attributed to slower dissociation of branches aged in buffer with 25 mM phosphate allowing time for them to be stabilized by binding to the slide coated with NEM-myosin anchors. However, that study did not measure time course of the dissociation of branches, and I did not compare the rate of branch formation on ADP and ADP-P_i mother filaments, so it unknown if the sources of Arp2/3 complex, the presence of NEM-myosin anchors on the surface or other factors account for the apparent difference.

Since the debranching kinetics are independent of the nucleotide (i.e. ADP or ADP-P_i or AMPPPNP) bound to the mother and daughter filaments, the stabilization of branches by BeF_x (Fig. 3B-D) is likely due to BeF_x bound to Arp2/3 complex in the branch junction. This suggests that the ADP-P_i-Arp2/3 complex intermediate has

different mechanical properties than the ADP-Arp2/3 complex after phosphate dissociation. The lack of an effect of 20 mM phosphate on debranching (Fig. 7) is consistent with the affinity of *S. pombe* ADP-Arp2/3 complexes in branch junctions for phosphate being very weak (K_d > 20 mM).

Force promotes but beryllium fluoride (BeFx) inhibits debranching by GMF.

Glia maturation factor (GMF) (29, 43, 44) promotes the dissociation of actin filament branches without applied force, so I measured how the concentration of fission yeast GMF influences the rates of dissociation of actin filament branches with ADP-BeF_x-Arp2/3 complex or ADP-Arp2/3 complex at a low buffer flow rate (15 µL min^{-1}). This flow rate exerts very little force on branches and had little or no effect on debranching (Fig. 3).

Concentrations of GMF up to 1 µM did not dissociate branches with ADP-BeF_x-Arp2/3 complex, but nanomolar concentrations of GMF promoted dissociation of branches with ADP-Arp2/3 complex (Fig. 8A). Time courses of dissociation of branches with ADP-Arp2/3 complex followed single exponentials (Fig. 8A) with lifetimes (τ_{obs}) that depended hyperbolically on the concentration of GMF (Fig. 8B).

Force increased the rate that GMF dissociated branches with ADP-Arp2/3 complex (Fig. 9), but dissociation was slower than predicted if GMF and force increased the rate of dissociation independently (i.e. their energetic contributions to debranching were additive). This raises the possibility that the reactions catalyzed by force and GMF are coupled and/or that debranching follows different pathways in the presence absence of force.

2.4 Figures and tables

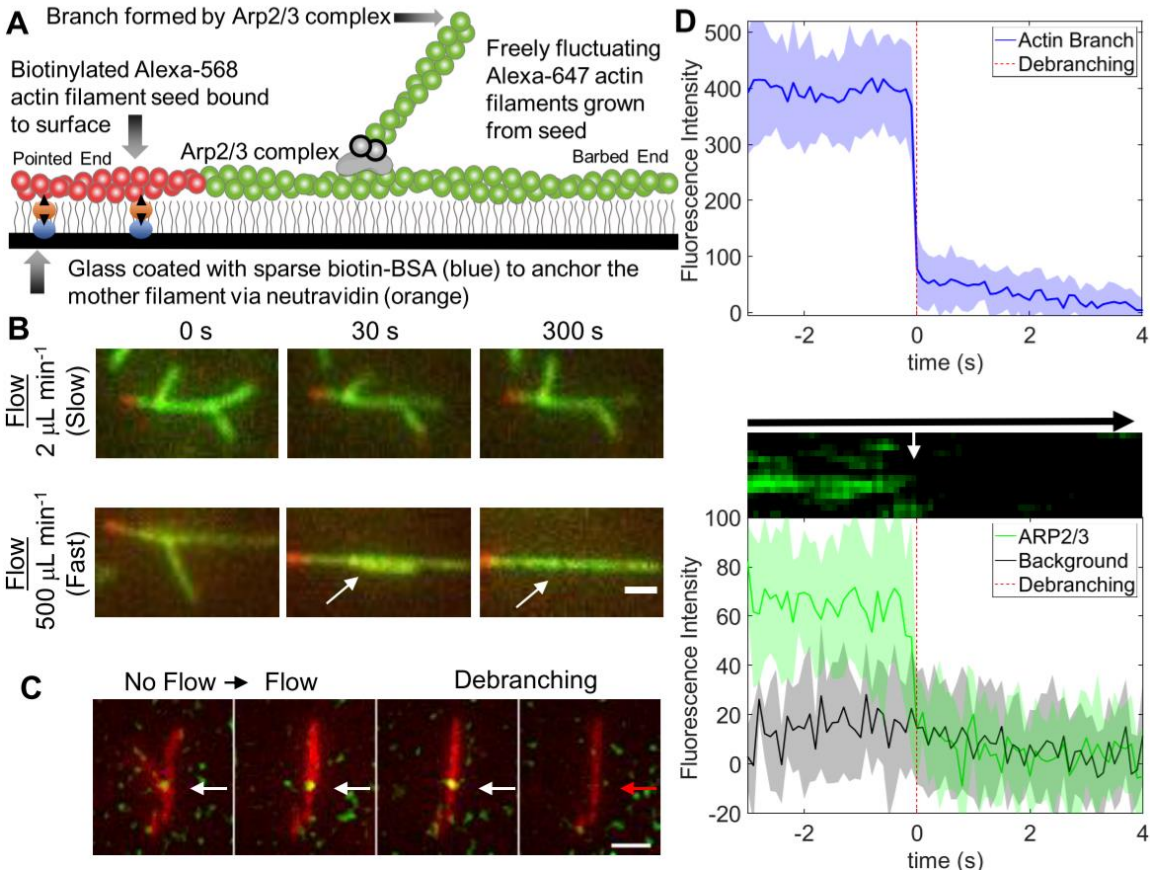

Fig. 1. Microfluidics assay to measure Arp2/3 complex debranching under force.

(A) Diagram showing a short segment of an actin filament containing 10% biotinylated and 15% Alexa568-labeled (red) actin subunits immobilized on the neutravidin-coated surface. The surface is passivated with 0.2% tween (illustrated with gray vertical lines). This seed was elongated at its barbed end with 1.5 µM 15% Alexa647-labeled Mg-ATP-actin (green) and Arp2/3 complex formed a branch with Alexa647-labeled Mg-ATP-actin. The green filaments fluctuate freely and are subject to viscous drag forces applied by fluid flow. *(B)* TIRF microscopy images of representative branched filaments under slow flow (2 µL min^{-1} ~0.004 pN of force for a 1.5 µm branch; top) and fast flow (500

μL min^{-1}, approximately 1.02 pN of force for a 1.5 μm branch; bottom). Branches are aligned in the direction of flow. The scale bar is 1 μm. *(C)* The Arpc5 subunit of the Arp2/3 complex was labeled with Alexa488 via Snap tag and tracked during debranching. The top panel shows time-lapse images with the actin filaments represented in red and the Alexa488-Arp2/3 complex located at the junction of the daughter branch and mother filament represented in green. *(D)* The top panel shows the spatially integrated fluorescence intensity of actin at a branch junction as a function of time, used to determine the observed debranching event time (t = 0). Middle panel shows a kymograph measured across a branched actin filament. Bottom panel shows the time course of spatially integrated fluorescence intensity of Arpc5 subunit at a branch junction with time aligned to its corresponding actin frame. The fluorescence intensity from Arp2/3 complex reproducibly decreased in a single step for all 12 debranching events observed.

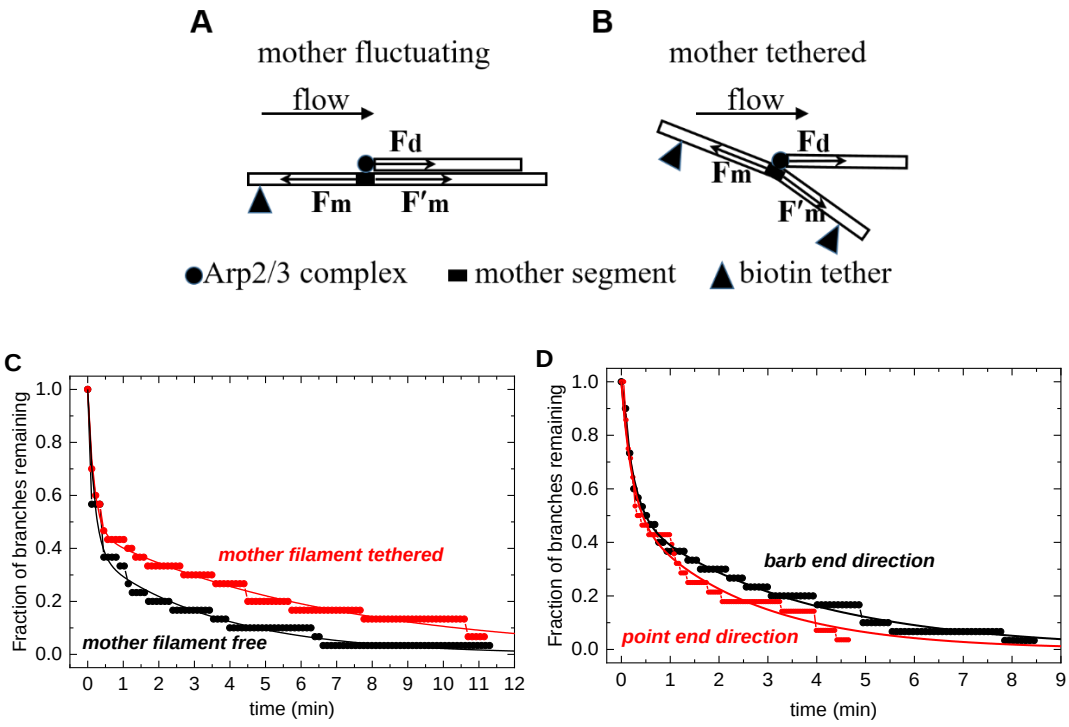

Fig. 2. Time courses of debranching depend weakly on tension in the mother filament and the direction of force.

A and B. Free body diagram illustrating the forces acting on a mother filament segment (filled rectangular block) with a bound daughter filament. One force ($\mathbf{F_d}$) originates from pulling of the freely moving daughter filament. This force in the direction of flow scales with the daughter filament length and flow rate (Eq. 5). The other two forces originate from pulling of the flanking mother filament segments at each side ($\mathbf{F_m}$ and $\mathbf{F'_m}$) of the branch. For a freely fluctuating mother filament, $\mathbf{F_m}$ and $\mathbf{F'_m}$ align with the flow direction, but in opposite directions (A). When the entire mother filament is tethered, the orientations of $\mathbf{F_m}$ and $\mathbf{F'_m}$ are confined and do not align with flow. The amplitudes of $\mathbf{F_m}$ and $\mathbf{F'_m}$ vary with geometry (B). The tension induced in the mother filament segment with a branch must counter-balance all the three forces acting on it. C and D. Branched

actin networks were assembled for 4 min with the entire mother filament or just a pointed end segment tethered to the surface. Without additional aging, the time courses of debranching followed double exponentials (n = 30 branches) under 500 μL min^{-1} buffer flow (~1.02 pN of force for a branch of 1.5 μm). C. Time courses of branch dissociation from tethered and freely fluctuating mother filaments with the buffer flow at 500 μL min^{-1}. The smooth lines through data are the best double exponential fits, yielding fast phase lifetimes of 0.19 (±0.02; free) and 0.18 (±0.01; tethered) min, amplitudes of 18 vs. 16%, and slow phase lifetimes of 3.5 (±0.2; free) and 6.8 (±0.2; tethered) min. The uncertainties represent the standard deviations from the fits. The force on immobilized mother filaments depends on their (random) orientations, while freely-fluctuating mother filaments align with flow and experience tension in a single direction. Thirty branches were scored for both free and tethered mother filament conditions. D. Time courses of branch dissociation with the buffer flow at 500 μL min^{-1} towards the barbed or pointed ends of mother filaments oriented parallel to the direction of flow and tethered to the surface throughout their lengths. Flow toward the mother filament barbed end pushed branches "forward", while flow towards the mother filament pointed end pushed branches "backward". n =30 for the barbed end direction and n =28 for the pointed end. See Movie S6-7). The smooth lines through data are the best fits to double exponentials, yielding fast phase lifetimes of 0.23 (±0.02; barbed) and 0.22 (±0.02; pointed) min, amplitudes of 49 vs. 48%, and slow phase lifetimes of 3.5 (±0.1; barbed) and 2.4 (±0.1; pointed) min. The uncertainties represent the standard deviations from the fits.

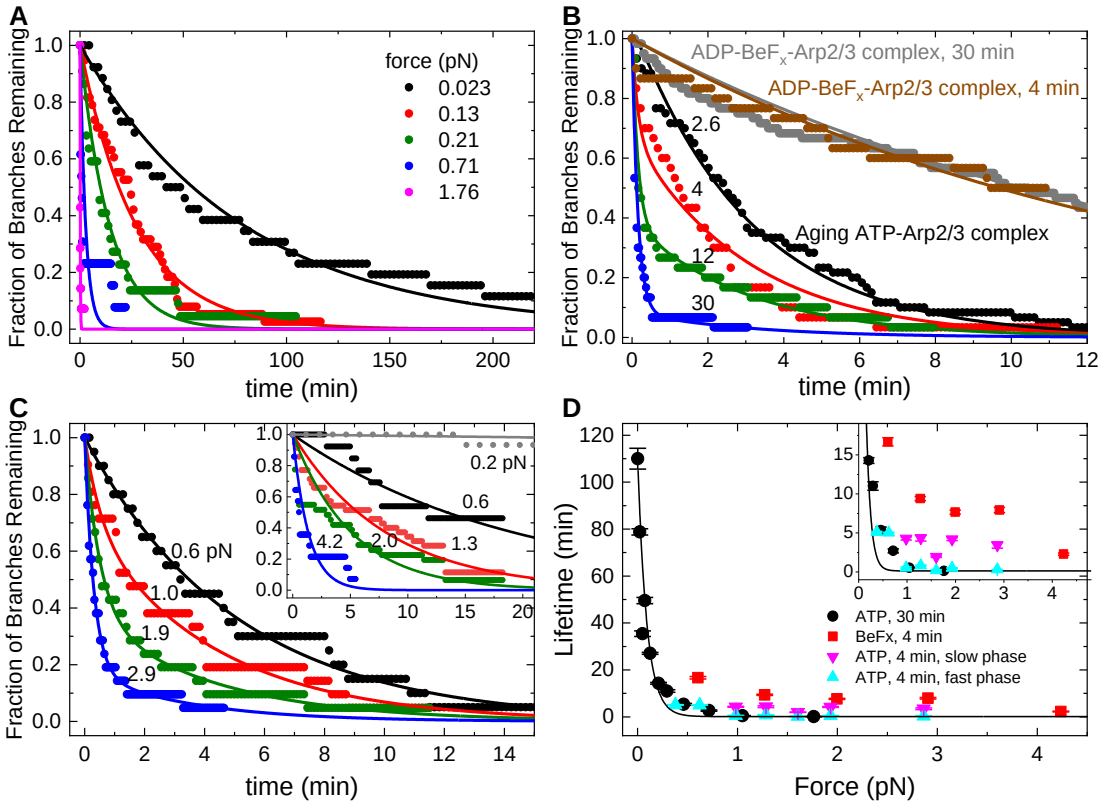

Fig. 3. Effects of mechanical force and nucleotide bound to Arp2/3 complex on the time course of dissociation of actin filament branches.

Arp2/3 complex branches were assembled in the flow chamber before applying flow as described in the *Materials and Methods*. In Panels A and C, the force on each observed branch was calculated from its length and the flow rate, and then binned at the indicated average forces values (see *Materials and Methods).* (A) The effect of force on the time course of dissociation of actin filament branches formed by ATP-actin monomers and ATP-Arp2/3 complex and aged for 30 min, when most branches had ADP bound to Arp2/3 complex. The fraction of branches remaining is plotted. Smooth curves are the best fits of single exponentials to the data. Each trace includes at least 14 branches. (B) Dependence of the time course of dissociation of branches formed with ATP-actin monomers and ATP-Arp2/3 complex with different aging times (2.6, 4, 12, 30 min) and

the presence of BeF_x. For all time courses, 500 μL min^{-1} of buffer flow was applied to the branches for debranching, producing a force of ~1 pN for a branch of 1.5 μm. The force on each branch was not calculated for the data shown. Smooth curves are the best global fits of double exponentials to the data for aging branches and yielded two shared rate constants for debranching: slow $k_{s,F}$ = 0.32 (±0.005) min^{-1} and fast $k_{f,F}$ = 6.67 (±0.44) min^{-1}. Smooth curves are the best single exponential fits to the data for branches aged 4 and 30 min with BeF_x with lifetimes of 13.9 (±0.2) min^{-1} for the sample aged ~4 min and 14.8 (±0.09) min^{-1} for the sample aged 30 min. Fig. 10C presents the fractional amplitudes obtained from the double exponential fits. (C) The effect of force on the time course of the dissociation of actin filament branches formed by ATP-actin monomers and ATP-Arp2/3 complex and aged for ~4 min using the same data collection and analysis methods as (A). The smooth curves are best fits of the data to single ($F \leq 0.6$ pN) or double exponentials ($F > 0.6$ pN). The fractional amplitude of the slow phase in the time courses that follow the double exponentials are 0.71 ±0.05 (F = 0.98 pN), 0.39 ±0.06 (F = 1.29 pN), 0.81±0.05 (F = 1.60 pN), 0.38 ±0.02 (F = 1.93 pN), 0.17 ±0.02 (F = 2.86 pN). Each trace includes at least 19 branches. Inset - Time courses of branch dissociation under a range of forces for branches formed from ATP-Arp2/3 complex in the presence of 2 mM BeF_x and aged ~4 min. Each trace includes at least 13 branches. The smooth curves are single exponential fits to the time courses. Branches dissociate slowly under 0.2 pN of force, so the debranching time course cannot be reliably fitted to obtain the branch lifetime. (D) Dependence of branch lifetimes on force for four different conditions: (filled black circles) branches formed from ATP-Arp2/3 complex and aged for 30 min to form branches with ADP-Arp2/3 complex (time courses in Panel A); (filled red squares)

branches formed from ADP-BeFx-Arp2/3 complex and aged ~4 min (time courses in Panel C inset); (filled pink triangles) slow debranching phase of branches formed from ATP-Arp2/3 complex and aged for ~4 min (ADP-P_i branch population; time courses in Panel C); and (filled blue triangle) fast debranching phase of branches formed from ATP-Arp2/3 complex and aged for ~4 min (ADP branch population; time courses in Panel C). The uncertainty bars for all data represent the standard deviations from the fits to exponentials shown in panels A and C. The smooth black curve is the best single exponential fit (Eq. 1) to the ADP-Arp2/3 complex debranching data points, yielding a half-force ($F_{1/2}$) of 0.054 (± 0.008) pN and branch lifetime in the absence of force (τ_0) of 106 (± 8) min (observed rate constant = τ_0^{-1} = 0.01 (± 0.007) min^{-1}). Inset shows that (a) fast phase lifetimes (blue triangles; 0.3 – 0.8 min at F > 1 pN) differ from the slow phase lifetimes (pink triangles; 2-4 min at F > 1 pN; t = 6.85, one tail $t_{critical}$ = 2.13 and p = 0.001 by Welch's unequal variances t-test); (b) the slow phase lifetimes (pink triangles; 2-4 min at F > 1 pN) differ from the debranching lifetimes with BeF_x (red squares; 8-9 min at F > 1 pN; t = 6.65, one tail $t_{critical}$ = 2.02 and p = 0.0006 by Welch's unequal variances t-test); and (c) that the fast phase lifetimes (blue triangles) do not differ significantly from the debranching with ATP aged 30 min lifetimes (black circles) at F > 1 pN (t = -0.86, two tail $t_{critical}$ = 2.45 and p = 0.42 by Welch's unequal variances t-test).

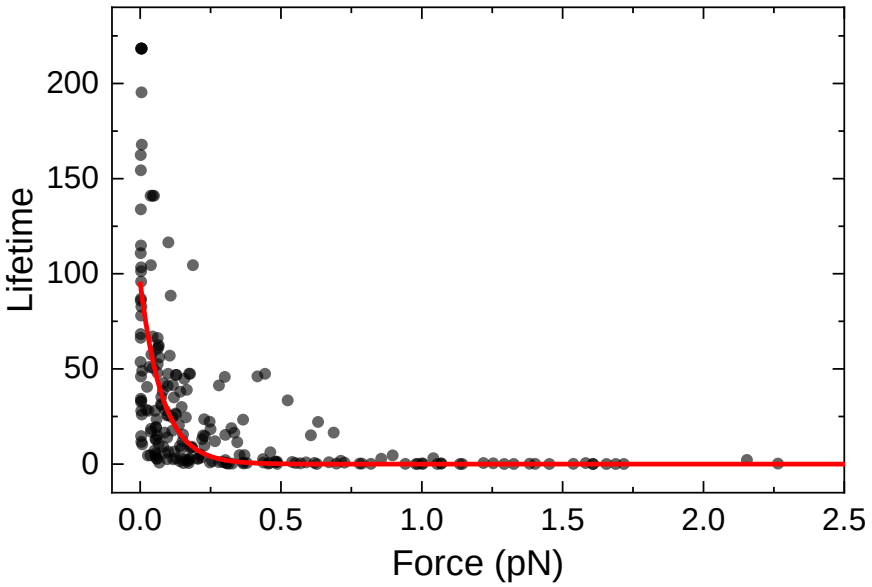

Fig. 4. Rug plot of ADP-Arp2/3 complex branch lifetimes

Rug plot analysis of dependence of branch lifetimes on force for branches formed from ATP-Arp2/3 complex and aged for 30 min to form branches with ADP-Arp2/3 complex (time courses in Fig. 3A). Force dependence of individual branch lifetimes was fitted to Bell's equation (Eq. 1) for comparison. The best fit resulted in characteristic distance d = 52 (± 7) nm (F1/2 = 0.054 (± 0.008) pN) and branch lifetime with 0 force τ_0 = 96 (± 6) min (rate constant = τ_0^{-1} = 0.01 (± 0.007) min^{-1}).

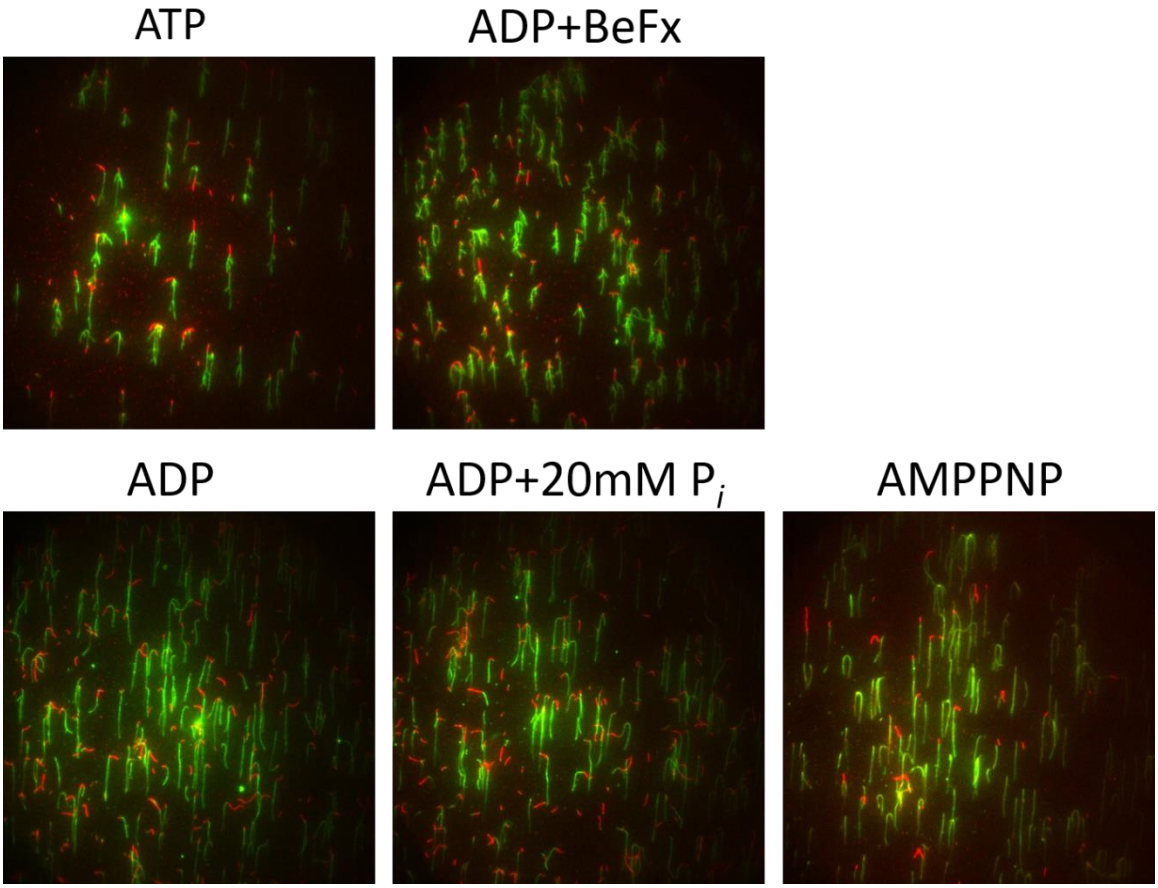

Fig. 5 Fluorescence micrographs of actin filaments in the presence of Arp2/3 complex in the flow chamber.

Experimental set-up and fluorescent labeling are as described in Fig 1A. The flow rate is ≤25 μL min^{-1}. Upper row: ATP-actin and ATP-Arp2/3 complex (ATP) and ADP-actin ADP-BeF_x-Arp-2/3 complex (ADP+BeFx) prepared from ADP-Arp2/3 with 2 mM $BeSO_4$ + 10 mM NaF robustly form branches. Lower row: Neither ADP-actin and ADP-Arp2/3 complex, with or without 20 mM P_i (ADP, ADP+20 mM P_i), nor AMPPNP-actin and AMPPNP-Arp2/3 complex (AMPPNP) form branches under the experimental conditions.

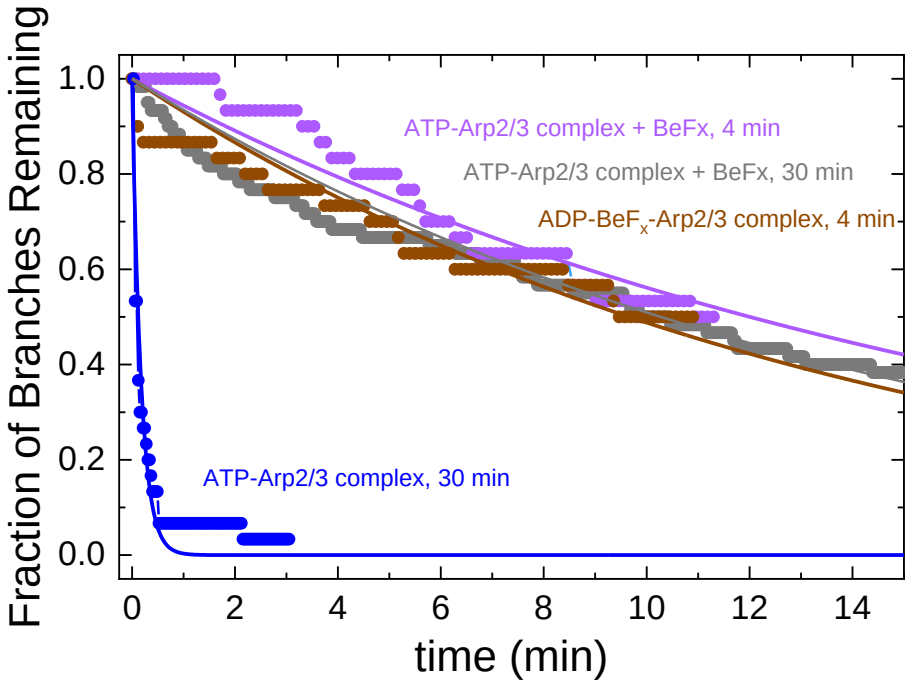

Fig. 6. Dissociation time courses of branches formed from ATP- or ADP-Arp2/3 complex in the presence or absence of BeF_x and aged for various times.

Debranching was observed under force by applying 500 µL min^{-1} (approximately 1.02 pN for a branch of 1.5 µm). All time courses follow single exponentials with observed lifetimes of 0.21 (±0.02) min^{-1} for ATP-Arp2/3 complex aged for 30 min (blue), 13.9 (±0.2) min^{-1} for ADP-Arp2/3 complex in the presence of 2mM BeF_x and aged for 4 min (brown), and 17.3 (±0.03) min^{-1} and 14.8 (±0.09) min^{-1} for branches formed with ATP-Arp2/3 complex in the presence of 2mM BeF_x and aged for 4 min (purple) or 30 min (gray), respectively.

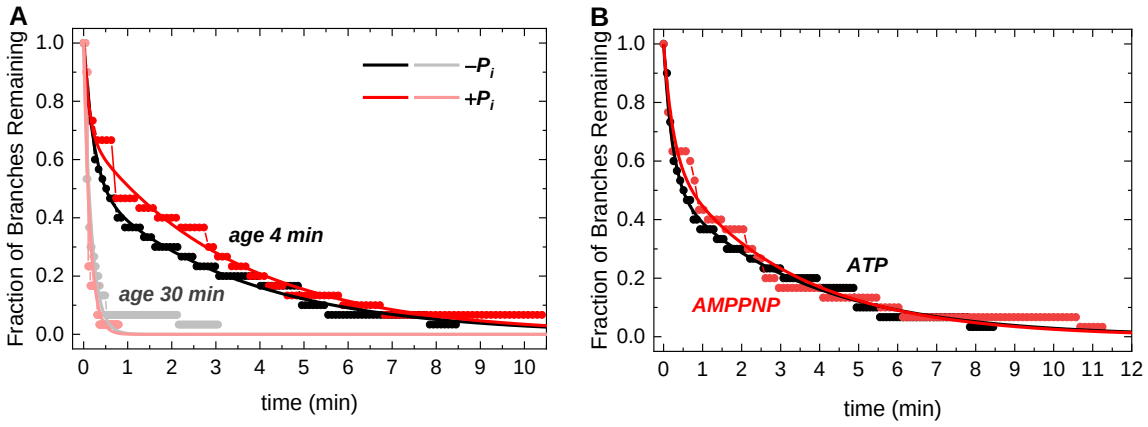

Fig. 7. The time course of debranching does not depend on the nucleotide state of the mother filament.

(A) Comparison of the time courses of dissociation of branches assembled in polymerization buffer containing 0.2 mM ATP with 0 or 20 mM potassium phosphate and aged for 4 min (dark colored traces) or 30 min (light colored traces) before observing the time course of branch dissociation at a buffer flow of 500 μL min^{-1} (approximately 1.02 pN of force for a branch of 1.5 μm). Phosphate (20 mM) saturates ADP-actin filaments to form ADP-P_i actin mother and daughter filaments. The affinity of ADP-Arp2 or Arp3 in branch junctions for phosphate is not known. *n* = 30 for all traces. The smooth lines through data are the best double exponential fits (4 min aging, fast phase lifetime = 0.23 (±0.02; –P_i) and 0.12 (±0.02; +P_i) min, amplitude %0.47 vs. 0.3% for +/- phosphate respectively and slow phase lifetime = 3.5 (±0.1; –P_i) and 3.3 (±0.1; +P_i) min) or single exponential (30 min aging; lifetime = 0.17 (±0.01; –P_i) and 0.14 (±0.01; +P_i) min). The uncertainties represent the standard deviations of the best fits of the data to single or double exponentials. (B) Comparison of the time courses of dissociation of branches assembled from ATP-Arp2/3 complex and ATP- or AMPPNP-actin monomers in

polymerization buffer with 0.2 mM ATP or AMPPNP. After aging branches for 4 min force was applied by buffer flowing at 500 μL min^{-1}. *n* = 30 branches for both conditions. The smooth lines through data are the best double exponential fits with slow phase lifetime of 3.5 (±0.1; ATP) vs. 3.2 (±0.1, AMPPNP) min and fast phase lifetime of 0.23 (±0.02; ATP) vs. 0.25 (±0.04, AMPPNP) min. The fast phase amplitude is 0.49 vs. 0.4%. The uncertainties represent the standard deviations of the best fits of the data to double exponentials.

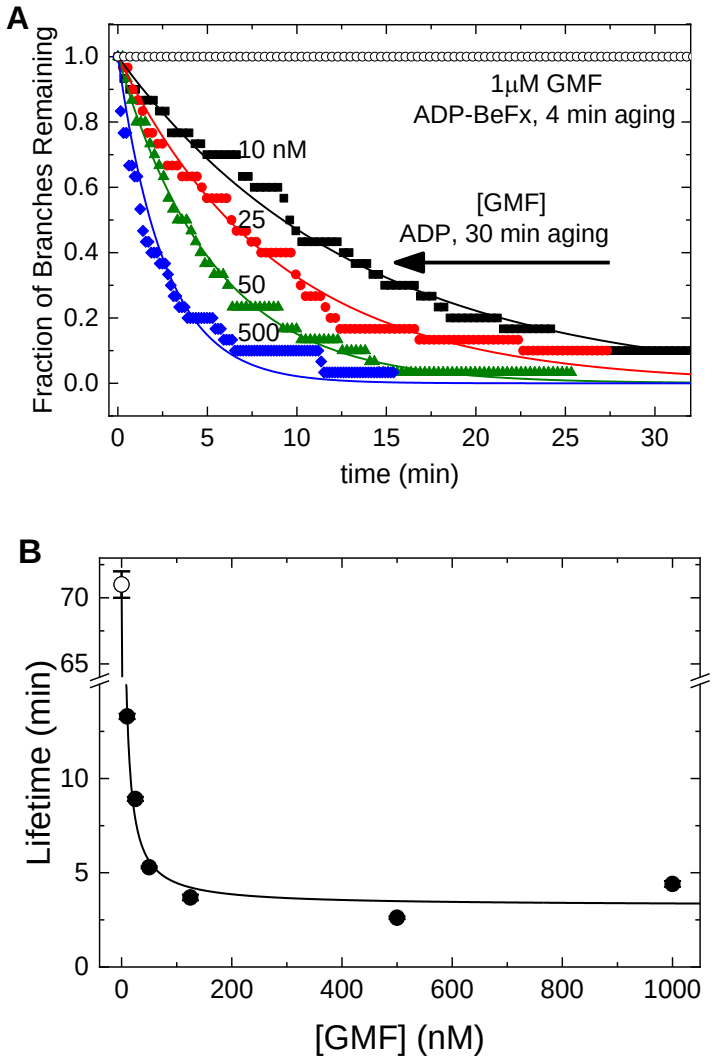

Fig. 8. BeFx inhibits debranching by GMF.

(A) Dependence of the time course of dissociation of branches with ADP-BeF_x-Arp2/3 complex or ADP-Arp2/3 complex on the concentration of GMF. Branches with ADP-BeF_x-Arp2/3 complex were assembled in buffer containing 0.2 mM ATP, 2 mM $BeSO_4$ and 10 mM NaF and aged for 4 min. Branches with ADP-Arp2/3 complex were assembled in buffer with 0.2 mM ATP and aged for 30 min to allow for ATP hydrolysis and phosphate dissociation (Fig. 3B). Debranching was initiated by flowing buffer with GMF at 15 μL min^{-1} and continued throughout the debranching measurements. The

smooth curves are the best fits of single exponentials to the data, yielding the (average) branch lifetimes. n = 30 branches for each trace. A concentration of 1 μM GMF did not dissociate branches with ADP-BeF_x-Arp2/3 complex assembled from ATP-actin and ATP-Arp2/3 complex with BeF_x and aged for 4 min (open black circles). *(B)* Dependence of the lifetimes of branches with ADP-Arp2/3 complex on the concentration of GMF at a buffer flow rate of 15 μL min^{-1}. The line is the best fit of Eq. 3 to the data, yielding a GMF binding affinity ($K_{d,GMF}$) of 40 (±10) nM and a maximum debranching rate constant ($k_{diss,GMF}$) of 0.31 (± 0.05) min^{-1}. At this low flow rate, branches with ADP-Arp2/3 complex (without GMF) dissociated with a rate constant ($k_{diss,0}$ = 0.014 ±0.0002 min^{-1}, indicated by an open circle) similar to that under zero force (Fig. 3B, Table 1)). The uncertainty bars are within the data points and represent the standard deviations of lifetimes in the best single exponential fits of times traces in Panel A.

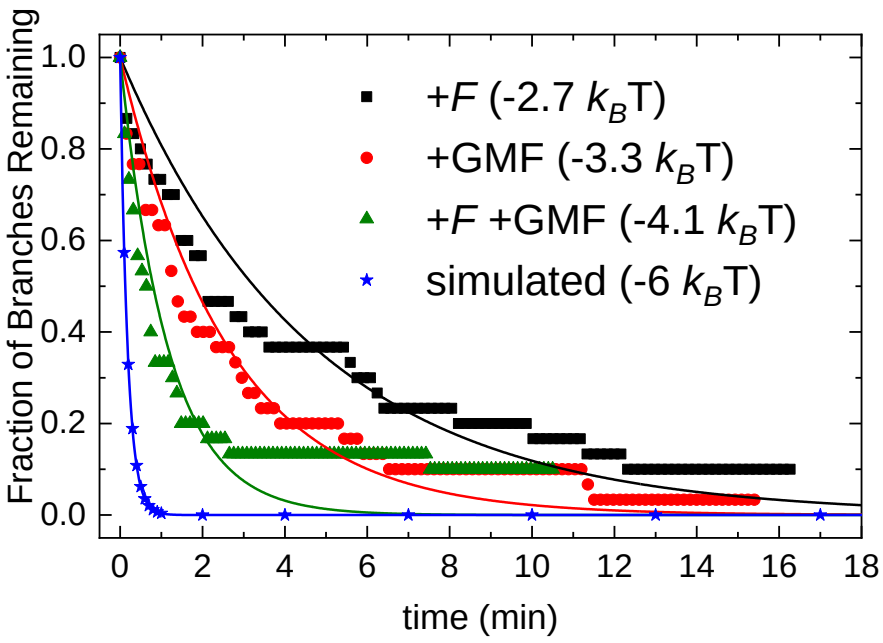

Fig. 9. Force and GMF together accelerate debranching of ADP-Arp2/3 complex branches more than either does alone.

Branches were formed as described in *Methods* and aged for 30 min to form ADP-Arp2/3 complex branches. Debranching was then initiated with 15 (very weak force – approximately 0.03 pN for a 1.5 μm branch) or 125 μL min^{-1} (moderate force – approximately 0.25 pN for a 1.5 μm branch) flow with and without 500 nM GMF. Those time courses follow single exponential decays (Fig. 3A). Debranching of ADP-Arp2/3 complex branches under 125 μL min^{-1} flow was ~15-fold faster than under 15 μL min^{-1} flow (lifetime reduced from 71 to 4.7 min, filled black squares), corresponding to a reduction in debranching activation energy of 2.7 k_BT ($\Delta\Delta G^{\ddagger} = k_B\mathrm{T}\ \ln(\tau_2/\tau_1)$. Inclusion of 500 nM GMF alone accelerated ADP-Arp2/3 complex branch debranching ~27 fold compared to that under weaker flow (15 μL min^{-1}) without GMF (lifetime from 71 to 2.6 min, filled red circles) and reduced the debranching activation energy by 3.3 k_BT. Force

(125 μL min^{-1} flow) and GMF (500 nM) together further accelerate debranching of ADP-Arp2/3 complex branches, shortening the lifetime from 71 to 1.16 min (filled green triangles), corresponding to a reduction in debranching activation energy of 4.1 k_BT. This reduction in debranching activation energy less than the sum of 6 k_BT predicted if the effects of force and GMF were additive. A simulated debranching time course with an activation energy reduction of 6 k_BT with corresponding lifetime of 0.18 min is shown for comparison (filled blue stars). The uncertainties were propagated from standard deviation in the lifetime obtained from the best exponential fits.

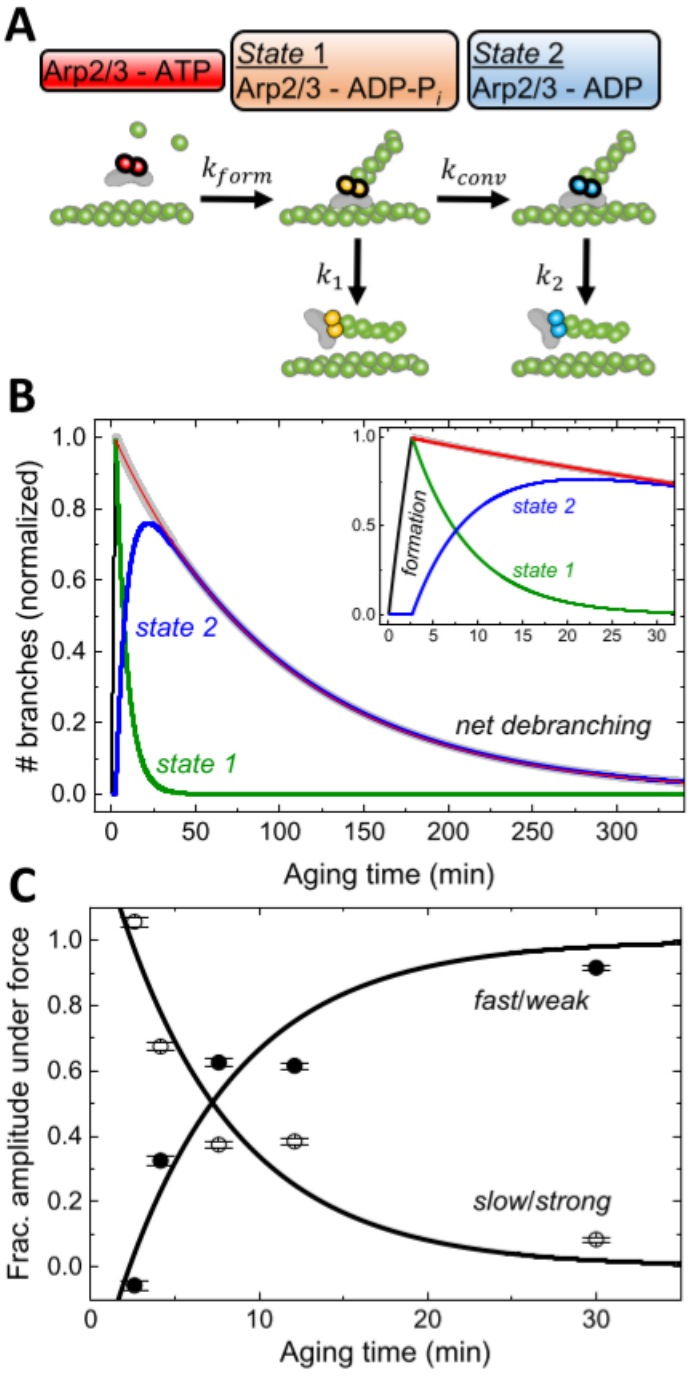

Fig. 10. Model and simulations of the pathways of branch formation, aging and debranching.

(A) Schematic of the hypothesis and model. Formation of a branch by ATP-Arp2/3 complex (red) is coupled to hydrolysis of ATP bound to the Arps (15, 17) with rate

constant k_{form}, yielding ADP-P_i-Arp2/3 complex (orange) in state 1. Irreversible phosphate dissociation with rate constant k_{conv} converts state 1 to ADP-Arp2/3 complex (blue) in state 2. Branches dissociate from mother filaments with rate constants k_1 for state 1 and k_2 for state 2, both sensitive to force. *(B)* Simulated time course of the model showing how the populations of state 1 branches, state 2 branches and dissociated branches evolve over time in the absence of force. I assumed that Mg-ATP-actin monomers and Mg-ATP-Arp2/3 complex formed branches for 2.6 min, when the free proteins were removed, and the reactions continued without additional branch formation. The red line represents the best single exponential fit to the observed debranching (i.e. combined from both states) starting with a normalized value of 1 at the end of branch formation (2.6 min). The experimentally determined or estimated rate constants used in the simulation are $k_{form}[Arp] = 0.12\ min^{-1}$, $k_{conv} = 0.14\ min^{-1}$, $k_1 = 0.012\ min^{-1}$ and $k_2 = 0.01\ min^{-1}$. *(C)* Aging time dependence of the fractional the slow and fast phase amplitudes in the debranching time courses under 500 µL min^{-1} of buffer flow, obtained from double exponential fits to the time courses (Fig. 3B). These data were used for extraction of fundamental rate constants in Table 1. The best global fits of the two-state model (Eq. 2) to the fractional amplitude data gave rate constants for conversion k_{conv} of 0.14 min^{-1}, state 1 branch dissociation k_1 of 0.012 s^{-1} and branch formation $k_{form,}$ of 0.02 $\mu M^{-1}\ s^{-1}$ without force (Table 1). The one negative fast phase amplitude at 2.6 min results from a net increase in the state 2 branch population during debranching under force after 2.6 min aging time. The state 2 branch population is the net sum of depletion from debranching (negative contribution to population, exponential decay) and gain from conversion of state 1 branches (positive contribution, exponential rise). For short aging

times, little or no state 2 branches exist for depletion and the conversion from state 1 branches, represented by an exponential rise (negative amplitude), dominates the time course (52, 53). The uncertainty bars are standard deviations of the fractions of branches from the global double exponential fits of debranching time courses with different aging times in Fig. 3B.

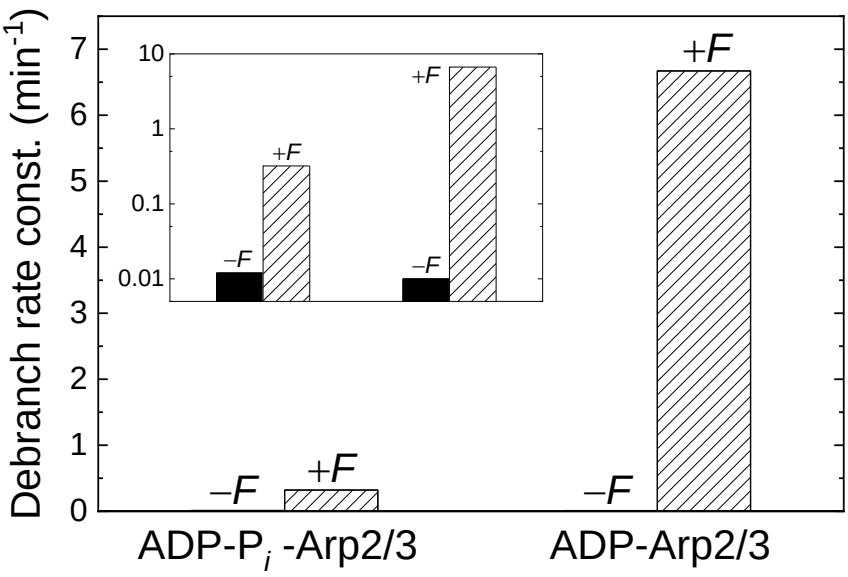

Fig. 11. Branches with ADP-Arp2/3 complex are far more sensitive to debranching by force than ADP-P$_i$-Arp2/3 complex.

The debranching rate constants in the absence of force for ADP-P$_i$-Arp2/3 complex (k_1) and ADP-Arp2/3 branches (k_2) were determined from analysis of data in Fig. 3 (Table 1). The global double exponential fits of the aging time-dependence of debranching time courses (Fig. 3B) yielded the observed slow ($k_{s,F}$) and ($k_{f,F}$) phase rate constant under 500 μL min^{-1} flow force. The rate constant for ADP-Arp2/3 complex debranching under force ($k_{2,F}$) is the fast, observed rate constant (i.e. $k_{2,F} = k_{f,F}$), whereas the slow observed rate constant represents a composite of the rate constants for ADP-P$_i$-Arp2/3 complex debranching ($k_{1,F}$) and conversion ($k_{conv,F}$) under force (i.e. $k_{s,F} = k_{1,F} + k_{conv,F}$; Eq. S41). Accordingly, $k_{1,F}$ can be estimated as $k_1 \leq k_{1,F} < k_{s,F}$. The upper limit, where $k_{1,F} = k_{s,F}$, is plotted. The actual $k_{1,F}$ value under force is therefore smaller than plotted. Note that the y-axis of the inset is on a logarithmic scale.

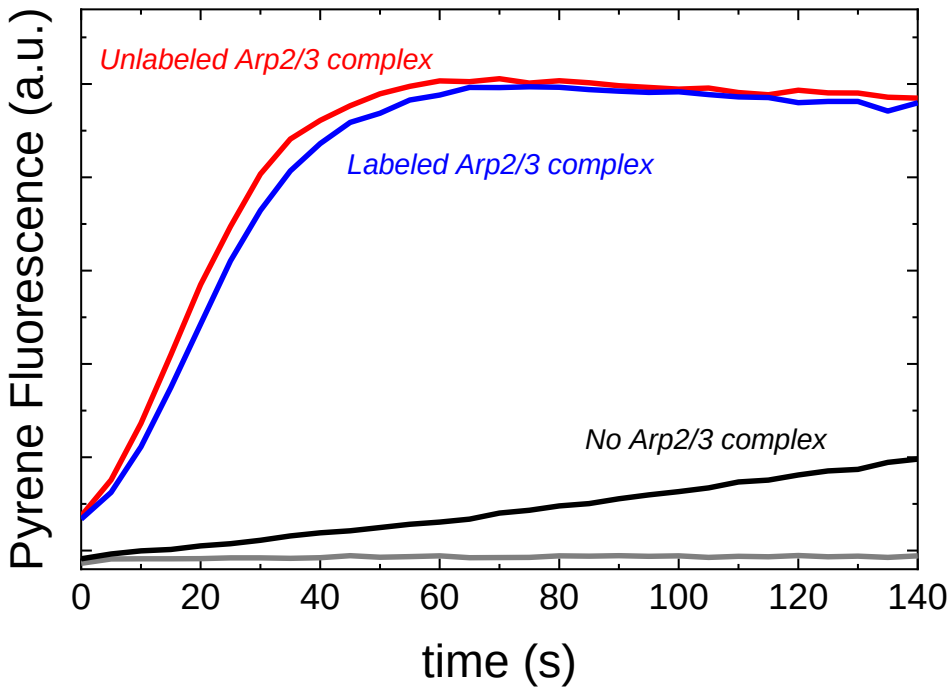

Fig 12. Comparison of the nucleation activity of labeled Arp2/3 complex.

Arp2/3 was labeled with an Alexa-488 conjugated to a snap tag on the Arpc5 subunit and nucleation activity was monitored by the time course of pyrenyl-actin polymerization. Conditions: 3 µM actin monomers (30% pyrene labeled), 200 nM Arp2/3 complex (± 82% Alexa-488 labeled), and 500 nM GST-VCA at 25 °C. Reactants were mixed at time zero and fluorescence emission was recorded at 407 nm (excitation wavelength = 365 nm) in a plate reader (Molecular Devices, SpectraMax GEMINI XPS). Red curve: unlabeled Arp2/3 complex in KMIE polymerization buffer; Blue curve: Alexa-488 Snap ArpC5 Arp2/3 complex in KMIE polymerization buffer; Black curve: 30% labeled pyrene monomers alone (no Arp2/3 complex) in KMIE polymerization buffer; Grey curve: 30% labeled pyrene actin monomers alone in low salt, non-polymerizing, G-buffer (54).

Table 1.

Table 1. Rate constants for branch formation and dissociation in the absence of force.

Conversion	State 1 debranching	State 2 debranching	Branch formation
k_{conv}	k_1 [a]	k_2 [b]	k_{form} [a]
(min^{-1})	(min^{-1})	(min^{-1})	(μM^{-1} s^{-1})
0.14±0.03	0.012	0.01±0.007	0.02
Fig. 4	Fig. 4	Fig. 2D	Fig. 4

a. The equations used to determine these parameters are approximations, so uncertainties are not reported.

b. From the fit of force dependent debranching data to Eq. 1, $k_2 = 1/\tau_0$. Fig. 2B. The error was calculated from the standard deviation τ_0 in the fit.

2.5 Discussion

Quantitative analysis of the two-state model for dissociation of actin filament branches.

The experiments presented here show that the nucleotide bound to Arp2/3 complex determines the sensitivity of branches to dissociation by physical force. A formal description of a simple two-state model (Fig. 10A) was used to analyze the data and estimate the rate constants for the three reactions and their sensitivities to force.

Description of the model.

The model (Fig. 10A) assumes that branches form when ATP-Arp2/3 complex binds to the side of a mother filament and nucleates a daughter filament growing at its barbed end. Hydrolysis of ATP in the active sites of *Acanthamoeba* Arp2/3 complex is closely associated with nucleation of the daughter filament (15, 17), so I assume that state 1 branches have Arp2/3 complex with bound ADP-P_i. Dissociation of the phosphate with a rate constant k_{conv} converts branch state 1 to branch state 2 with ADP bound to Arp2/3 complex. Branches in either state can dissociate from the mother filament. The model predicts that overall, net debranching time courses follow double exponentials with two rate constants. One observed rate constant is the sum of the rate constants for state 1 debranching and conversion ($k_{obs,1(F)} = k_{1(F)} + k_{conv(F)}$; ($F$) indicates optional force). The second observed rate constant corresponds to debranching of state 2 ($k_{obs,2(F)} = k_{2(F)}$; *SI Appendix* Eqs. S25 and S29). Force accelerates the dissociation of branches with either ADP- and ADP-P_i-Arp2/3 complex, but branches with ADP-P_i or ADP-BeF_x-Arp2/3 (mimicking the ADP-P_i state) complex are much more resistant to force than branches with ADP-Arp2/3 complex. As branches age, phosphate release converts slowly

dissociating, “young and strong” state 1 branches with ADP-P_i-Arp2/3 complex into rapidly dissociating, “old and weak” state 2 branches with ADP-Arp2/3 complex.

Formulation of the model.

The experimental data was analyzed by using a parallel debranching pathway (Figure 10A) where “young” (strong, state 1) branches convert to “old” (weak, state 2) branches as they age (Fig. 10A). The fit of aging time-dependence of the fractions of slowly and rapidly dissociating branches was observed under force as the amplitudes ($A_{s,F}$ and $A_{f,F}$, respectively; Fig. 10) of double exponential fits to the following functions:

$$A_{s,F} = \frac{be^{-\left(k_{conv}+k_1-k_2\right)\left(t_{age}-t_1\right)}}{1+ae^{-\left(k_1+k_{conv}-k_2\right)\left(t_{age}-t_1\right)}}$$
$$A_{f,F} = \frac{1+\left(a-b\right)e^{-\left(k_{conv}+k_1-k_2\right)\left(t_{age}-t_1\right)}}{1+ae^{-\left(k_1+k_{conv}-k_2\right)\left(t_{age}-t_1\right)}} = 1-A_{s,F} \qquad 2,$$

where t_1 is the 2.6 min during which branches formed from ATP-Arp2/3 complex and ATP-actin monomers, t_{age} is aging time, the intrinsic debranching rate constants are k_1 for state 1 and k_2 for state 2 in the absence of force and k_{conv} is the rate constant for conversion of state 1 to state 2 in the absence of force (Fig. 10A). The constants a and b are unitless composites of rate constants and initial branch concentrations defined below. The constant a is force independent and determined only by intrinsic debranching in the absence of an applied force. The constant b is a function of debranching and conversion

under force yielding force-dependent amplitudes ($A_{s,F}$ and $A_{f,F}$) when debranching and/or conversion are force-dependent.

$$a = \frac{\dfrac{k_2 - k_1}{k_2 - k_1 - k_{conv}}}{\dfrac{[branch_2]_{t_1}}{[branch_1]_{t_1}} - \dfrac{k_{conv}}{k_2 - k_1 - k_{conv}}}, \quad b = \frac{\dfrac{k_{2,F} - k_{1,F}}{k_{2,F} - k_{1,F} - k_{conv,F}}}{\dfrac{[branch_2]_{t_1}}{[branch_1]_{t_1}} - \dfrac{k_{conv}}{k_2 - k_1 - k_{conv}}}$$

Estimation of the rate constants for branch formation and phosphate dissociation. Global analysis of the data (Fig. 3B and 10C) yielded an overall pseudo first order association rate constant for branch formation of 0.12 min^{-1}. Given 100 nM Arp2/3 complex used in my experiments, an estimate of the second order association rate constant for Arp2/3 complex binding to mother filaments and subsequent activation (k_{form}) is ~0.02 μM^{-1} s^{-1} (Table 1), consistent with published reports (18, 19, 55).

The best fit of the fractional amplitudes to Eq. 2 (Fig. 4C) yielded a rate constant (k_{conv}) of 0.14 (±0.03) min^{-1} (corresponding to a lifetime of >7 min) for conversion of state 1 branches to state 2 branches. The rate of conversion reaction is interpreted as the release of P_i from the Arp2/3 complex, and thus state 2 branches as ADP-Arp2/3 complex branches. This rate constant inferred for P_i release from ADP-P_i Arp2/3 complex is similar to the rate constant of ~0.18 min^{-1} for P_i release from actin filaments (51).

I can place a limit on the rate constant for phosphate binding to ADP-Arp2/3 complex in a branch junction (k_{+Pi}). I interpret conversion to reflect P_i release, so k_{-Pi} = k_{conv} = 0.14 (±0.03) min^{-1}, and know that P_i binds Arp2/3 complex in branches with a low affinity (K_d >20 mM, Fig 7). Therefore, the second order association rate constant of k_{+Pi} is less than 7 M^{-1} min^{-1} = 0.12 M^{-1} s^{-1}. This value is two orders of magnitude slower than

P_i binding to ADP-actin subunits in the interior of filaments (600 $M^{-1}min^{-1}$ = 10 $M^{-1}s^{-1}$; (51)).

Estimation of the rate constants for branch dissociation at low force.

The rate constant for dissociation of state 2 branches at zero force is $k_2 \sim 0.01$ min^{-1}, based on the intercept of the force-dependence of ADP-Arp2/3 complex (state 2) branch lifetimes (Fig. 3D). The rate constant for debranching from state 1 at zero force (k_1) is ~0.012 min^{-1}, from the analysis of the aging time-dependence of time course of dissociation of branches (Figs. 3B and 10C, Table 1, see *SI Appendix* Part 2 Eq. S42). As a result of these two rate constants being similar ($k_1 \sim k_2$), debranching without force follows a single exponential with a rate constant of ~k_2 (*SI Appendix* Part 2 Eq. S25 and Fig. 10B), even though three reactions (conversion and debranching from state 1 and state 2) occur simultaneously.

Time courses also follow single exponentials at low forces (<0.6 pN), independent of the aging time (Fig. 3C & 3D). This behavior arises because dissociation is much slower than conversion ($k_1 << k_{conv}$), so ADP-P_i branches convert to ADP before dissociating. At forces >1 pN, the observed dissociation time courses follow double exponentials because $k_{conv} < k_1$ and debranching occurs from both ADP-P_i and ADP branches.

Estimation of the force sensitivity of the branch dissociation rate constants.

Force increases the dissociation rate constants of both branch states, but has a larger effect on state 2 branches with ADP-Arp2/3 complexes than state 1 branches with ADP-P_i-Arp2/3 complexes (Fig. 3D). The best global fits of the double exponential time courses at intermediate aging times yielded a ~20-fold difference in the lifetimes of the

species that dissociated slowly ($k_{s,F}$ = 0.32 (±0.005) min^{-1}) and rapidly ($k_{f,F}$ = 6.67 (±0.44) min^{-1}) at a buffer flow rate of 500 μL min^{-1} (Fig. 3B). Under this force, the observed fast rate constant is the rate constant for the state 2 branch dissociation (i.e. $k_{f,F} = k_{2,F}$) and the observed slow rate constant is the sum of the rate constants for dissociation for state 1 branches and conversion from state 1 to state 2 (i.e. $k_{s,F} = k_{1,F} + k_{conv,F}$; *SI Appendix* Part 2 Eqs.S29 and S41).

Force produced by a flow of 500 μL min^{-1} increased the observed dissociation of branches ~670-fold (from k_2 = 0.01 to $k_{2,F}$ = 6.67 min^{-1}) for those with ADP-Arp2/3 complex but only 32-fold (from k_1 = 0.012 to $k_{1,F} = k_{s,F} - k_{conv,F} < k_{s,F}$ = 0.32 min^{-1}; Fig. 3B and Fig. 7) for those with ADP-P_i-Arp2/3 complex. This difference in force sensitivity of the two states explains the dramatic acceleration in overall debranching with aging (Fig. 3B). Furthermore, the force produced by 500 μL min^{-1} flow is estimated to increase k_{conv} only two-fold from k_{conv} = 0.14 min^{-1} in the absence of force to $k_{conv,F} = k_{s,F} - k_{1,F} < k_{s,F}$ = 0.32 min^{-1} in the presence of force (Fig. 7.).

Implications of the force sensitivity of branches for their turnover in cells.

Implications for debranching by myosin motor proteins.

A sustained flow force of ~1 pN dissociates ADP-Arp2/3 complex branches in <30 s (Fig. 3D), raising the possibility that pN contractile forces generated by myosin motors could rapidly debranch and reorganize Arp2/3 complex networks. Myosin accelerates network disassembly and reorganization in both biomimetic systems (56, 57) and in cells (58, 59). The work (i.e. energy term) from the applied force determines the overall debranching acceleration, not the force per se.

Implications of nucleotide dependent force sensitivity of Arp2/3 complex debranching. "Young" branches with ADP-P_i-Arp2/3 complex are more resistant to dissociation by force than "old" branches with ADP-Arp2/3 complex. Nucleation promoting factors associated with membranes (plasma membrane, vesicles, intracellular bacteria) activate Arp 2/3 complex, so "young" branches are located closer to these surfaces than "old" branches. If force is uniformly distributed across the filament network, old branches farthest from the surface with nucleation promoting factors would be preferentially debranched.

This differential response to force may contribute to the observed remodeling of cellular branched actin networks under load, including local changes in branch density (30, 32, 38). A minimal kinetic model was applied (*SI Appendix Part 3, see paper in revision at PNAS*) to analyze how selective, force-sensitive debranching might influence the distribution of branches in actin networks at the leading edge of cells. The model assumes Arp 2/3 complex is activated uniformly at the membrane, such that the branch density distribution is also uniform, on average, along the plane parallel to the cell membrane at the leading edge. The model with the experimental parameters determined here predicts that the density of branches decays exponentially (see also (60-62)) along the axis perpendicular to the membrane, toward cell interior both in the absence and presence of force, but preferential debranching of old Arp 2/3 complexes shortens the branch density decay length and can, under some conditions, increase the local branch density near the membrane. Thus, external force on the leading edge of cells favors debranching of old branches that have migrated toward the cell interior over young branches still near the membrane and can thus contribute to spatial and vectorial network

turnover. External force may also influence binding of cofilin (33) and GMF (Fig 8; discussed below), both of which display debranching activity (43, 46).

GMF selectively dissociates ADP-Arp2/3 complex branches.

Fission yeast GMF increases the rate constant for dissociation of branches with ADP-Arp 2/3 complex up to ~20-fold, but does not dissociate branches with ADP-BeF_x-Arp 2/3 complex (Fig. 8). The following parallel reactions describe GMF-catalyzed dissociation of branches with ADP-Arp2/3 complex:

$$\begin{array}{ccc} Arp + GMF & \overset{K_{d,GMF}}{\rightleftharpoons} & Arp\text{-}GMF \\ \downarrow k_{diss,0} & & \downarrow k_{diss,GMF} \\ \multicolumn{3}{c}{debranched} \end{array} \qquad \text{Scheme 1,}$$

where $k_{diss,0}$ and $k_{diss,GMF}$ are the dissociation rate constants of branches formed by Arp2/3 complex alone (*Arp*) and GMF-bound Arp2/3 complex (*Arp-GMF),* and $K_{d,GMF}$ is the affinity of GMF for Arp 2/3 complex in a branch junction. This scheme assumes that GMF binding equilibrates rapidly compared to the rate of debranching (and $k_{+GMF}[GMF]$, $k_{-GMF} >> k_{diss,0}$, $k_{diss,GMF}$) and that [*GMF*]>>[*Arp2/3 complex*].

Debranching from the parallel pathway in Scheme 1 follows a single exponential (63). The dependence of the observed branch lifetime (τ_{obs}) on the concentration of GMF to Eq. 3 can be expressed in two ways, first:

$$\tau_{obs} = \tau_0 - \frac{(\tau_0 - \tau_{GMF})[GMF]}{K_{d,GMF}\left(\frac{\tau_{GMF}}{\tau_0}\right) + [GMF]} \qquad 3$$

Alternatively, the relationships can also be expressed in terms of observed rate constants (63, 64):

$$k_{obs} = k_0 + \frac{(k_{GMF} - k_0)[GMF]}{K_{d,GMF} + [GMF]} \qquad 4.$$

The best fit of Eq. 3 to the dependence of the observed branch lifetime (τ_{obs}) on the concentration of GMF (Fig. 8B) yielded an apparent affinity of GMF for ADP-Arp2/3 complex ($K_{d,\,GMF}$) of 40 (± 10) nM and a lifetime of GMF bound to ADP-Arp2/3 complex in branches (τ_{GMF}) of 3.3 (± 0.5) min. This corresponds to a debranching rate constant ($k_{GMF} = 1/\tau_{GMF}$) of 0.31 (± 0.05) min^{-1}. In Eqs. 3 and 4, k_0 is the debranching rate constant and τ_0 is the branch lifetime without GMF under very low flow rate (15 μL min^{-1}), i.e. very low average force. The best fit yielded $k_0 = 1/\tau_0 = 0.014$ (± 0.0002) min^{-1}, corresponding to $\tau_0 = 71$ (± 1) min. These values are slightly faster than the intrinsic dissociation rate constant for branches with ADP-Arp2/3 complex in the absence of force (>100 min; Fig. 8) due to the 15 μL min^{-1} flow rate employed in this experiment. The GMF concentration at half maximum effect is given by $K_{d,GMF}$ (τ_{GMF}/τ_0) in Eq. 3 and $K_{d,GMF}$ in Eq. 4, so its value differs depending on how the data is plotted.

Reported affinities of GMF for soluble Arp2/3 complex ($K_{d,GMF}$) vary widely: >>10 μM for ATP-Arp 2/3 complex (65); 0.7 μM for ADP-Arp2/3 complex (65); and 13 nM (29, 43, 44) or ~1 μM (66) for Arp2/3 complex without a specified nucleotide. *S. cerevisiae* (29, 43, 44); bovine brain (65); and *S. pombe,* this study and (66). I found that the measured affinity of GMF for Arp2/3 complex in branch junctions bound to both a mother and daughter filament depended on the bound nucleotide. Arp2/3 complex used in these studies came from different organisms.

Thus, GMF preferentially dissociates “old” branches with ADP-Arp2/3 complex rather than “young” branches with ADP-P_i-Arp2/3 complex. Given that GMF has a much lower affinity for ATP-Arp2/3 complex in solution than ADP-Arp2/3 complex (65) weak binding of GMF to ADP-P_i-Arp2/3 complex in branches is the most likely explanation

for the resistance of young branches and branches with ADP-Be$_x$-Arp2/3 complex to dissociation by GMF. The nucleotide bound to Arp2/3 complex might also affect the debranching reaction directly.

Saturating GMF destabilizes ADP-Arp2/3 complexes, reducing their lifetime from more than 60 min to ~3 min (Fig. 8). While GMF strongly promotes debranching, these long lifetimes (3 min) at saturating GMF concentrations place limits the role of GMF in mediating debranching and network turnover in cells. More rapid debranching may be achieved by combining GMF with force and/or from contributions from other debranching proteins such as cofilin, which dissociates branches on a second time scale at micromolar concentrations without force (46).

Arp2/3 complex likely dissociates with the daughter filament.

A daughter filament and its associated Arp2/3 complex dissociate simultaneously (within the 100 ms time resolution of the experiments) during debranching events. I cannot eliminate a pathway in which the daughter filament detaches first, followed by rapid release of Arp2/3 complex. However, I favor a mechanism where the interface between Arp2/3 complex and the mother filament ruptures and simultaneously releases the daughter filament with Arp2/3 complex on its pointed end. This mechanism is consistent with actin filaments rarely fragmenting under debranching conditions, so the rate constant for rupture of the actin-actin interface is hundreds of times slower than the rate constant for rupturing a branch junction. Given that the interface between Arp2/3 complex and the daughter filament is structurally similar on many levels to an actin-actin interface (67), it is likely to rupture slowly like actin. This assumes that the Arp2/3 complex is in its active conformation with Arp2 and Arp3 positioned similar to actin monomers in a filament.

2.6 Methods

Protein purification.

Rabbit skeletal muscle actin was purified from back and leg muscles and labeled on lysine residues with NHS esters of Alexa 568, Alexa 647, or biotin (68, 69) or on Cys 374 with pyrene iodoacetamide (54). Actin monomers with bound ATP were passed twice through a desalting column to exchange into G-Buffer (20 mM Tris pH 8, 2 mM $CaCl_2$, 10 mM NaN_3, 0.2 mM ATP, and 0.5 mM DTT) containing 0.2 mM AMPPNP instead of ATP and incubated for 1 h at 25 °C. Remaining free nucleotides were removed with a desalting column in G-Buffer containing AMPPNP instead of ATP prior to polymerization experiments. Arp2/3 complex was stored in ATP buffer solution composed of 10 mM PIPES at pH 6.8, 100 mM KCl, 1 mM $MgCl_2$, 0.25 mM EGTA, 0.1 mM ATP, and 1mM DTT.

Recombinant fission yeast GST-VCA was purified from bacteria (70). *S. pombe* Arp2/3 complex was purified from the TP150 strain, a protease deleted *S. pombe* strain as described in (70). A *S. pombe* strain with the Arpc5 subunit tagged with a snap tag was obtained from the Berro Lab. This Arp2/3 complex was purified as the WT Arp2/3 as described above except the last gel filtration step was omitted (until after labeling) to retain high yield required for labeling and DTT was replaced with 0.2mM TCEP. 488-Snap dye was purchased from NEB and resuspended in DMSO. This dye was mixed with the purified Arp2/3 Arpc5 snap tagged complex at a ratio of 3:1 and incubated for 4 hours rotating at 4 C°. Then the protein and excess dye were centrifuged in a TLA-110 for 20 min at 70K to remove any aggregated protein or dye. Excess dye was removed with three consecutive 5ml Hi-Trap desalting columns and gel filtered as described in (70). Bulk

polymerization assays with pyrenyl-actin and GST-VCA showed that Arp2/3 complex with 82% labeling of the snap tag nucleated 91% as many actin filaments as unlabeled Arp2/3 complex (4.2 nM vs 4.6 nM of barbed ends at half maximal polymerization; Fig. 12) ((54, 70).

A cDNA for *S. pombe* GMF was cloned and inserted into the pet28a plasmid that includes GST and TEV protease sites. Recombinant GMF was expressed in Rosetta2 BL21 *E. coli* cells (Novagen) and purified using glutathione affinity chromatography. After cleaving off GST with TEV-protease, a second round of glutathione chromatography removed the protease and GST. After FPLC on a MonoQ column (43), the GMF was greater than 95% pure when analyzed by SDS PAGE.

Microscopy and Microfluidics.

A TIRF microscopy system with a Till iMic digital microscope equipped with a ×100 objective NA=1.49 (Olympus) and an Andor iXon897 EMCCD camera was used in this study. Images were acquired at a rate of 5 to 30 frames per second. Coverslips were cleaned with the following solutions, all incubated in a sonicator for 30 min and rinsed intensively with Milli-Q water in between steps; 2% Hellmanex, water, acetone, 1 M HCl, 5 M KOH, and hexane, then silanized with 650 µL of dichlorodimethyl silane in 500 mL of hexane for 30 min, and subsequently rinsed and sonicated in hexane for 3 ×1 min. Coverslips were dried using a stream of nitrogen gas and stored in falcon tubes at –20 ^{o}C for up to 2 months (71).

A glass microfluidic chamber was constructed as described (72). Briefly, the input and output ports for flow solution were formed in PDMS using a flat tip needle. Holes connecting the PDMS to parallel sample chambers were drilled through the glass with a

diamond tip bit. Subsequently, a plasma cleaner was employed to bond PDMS to slide glass. Immediately before use, chambers were assembled using parafilm on the glass slide opposite to PDMS ports and a coverslip was placed over the parafilm and sealed with heat.

A fixed rate hydrodynamic flow exerted by an automatic syringe pump applied pulling forces on actin filaments. The magnitude of pulling force on a branch joint (**F_d**, Fig 2.A and B) scales with daughter filament branch length and flow rate. These values span a range up to a few pN for the daughter filament lengths and flow rates examined here. Pulling force was calculated according to the Batchelor (73) equation:

$$F_d = \eta \frac{2\pi l v}{\ln\left(\frac{2h}{r}\right)} \qquad 5$$

Equation 5 estimates drag force on a cylindrical filament with correction for the height (h) of the filaments from the surface of the flow chamber (74). Solution viscosity (η)is assumed to equal unity. l is the (daughter) filament length and varies for individual branches. The average actin filament radius is r = 4 nm, and v is the linear fluid velocity in the plane of the filament. I assume an average height (h) of 200 nm from the flow chamber surface. The fluid velocity (v) is proportional to bulk flow rate and was determined from the movement of 100 nM TetraSpek beads (Thermo Fisher) through the sample chamber (73). Only beads moving parallel to the surface were employed in my analysis, as the flow velocity profile changes with the height from the chamber surface. Bead flow velocity was measured via ImageJ “Manual Tracking” and used in force calculations (73). In the experiments presented in Fig 2A and 2C, multiple experiments at different flow rates were performed and the force on each branch was calculated using

the flow rate and length of the branch. Then, debranching data from different flow cells with a range of flow rates were binned according to the force on each branch and plotted as survival time courses, given by the fraction of branches remaining at each time point. For example, the branches in Fig. 2A were divided into bins of at least 13 branches. The bin size for each data point is approximately the mid-point between the point itself and its neighboring data points (Fig 2D). At low forces (0.002-0.4 pN), the bin sizes were small, for example (0-0.04 pN, 0.1-0.2 pN, etc) and higher forces (> ~1 pN) the bin sizes were larger for example (0.8-1.4 pN, 1.4-2.4 pN, etc).

Some of these parameters are uncertain, so the estimated force values may be offset systematically for all of my experiments. The least certain parameter is the distance of individual filaments from the surface, which may vary by <50% from the average distance of 200 nm assumed here. A 500 μL min^{-1} flow rate produces forces on a 1.5 μm branch of 0.94 pN at a height of 300 nm, 1.02 pN at 200 nm and 1.20 pN at 100 nm Therefore, the absolute forces and parameters calculated from them may be imprecise, but no more than 20%, and the relative forces between experiments can be compared.

Preparation of branched actin filament networks and experimental procedures.

KMIE buffer (24, 45) (10 mM imidazole pH 7.0, 50 mM KCl, 2 mM $MgCl_2$, 1 mM EGTA, 0.2 mM ATP, 2 mM DTT) supplemented with 15 mM glucose, 0.02 mg mL^{-1} catalase, and 0.1 mg mL^{-1} glucose oxidase was used for all microscope experiments, unless noted otherwise. Filaments of 568-Alexa-labeled actin (Fig. 1A, red filament segment; 15% labeled with Alexa-568 and containing 10% biotinylated actin subunits; were polymerized in KMIE buffer, sheared by vigorous pipetting, and subsequently

mixed with 1.5 μM 647-Alexa labeled actin monomers (Fig. 1A, green segment and branch), 0.1 μM Arp2/3 complex, and 0.5 μM GST-VCA in KMIE buffer. This solution was incubated for 1-2 min to initiate branch formation. During the branching reaction, green actin monomers elongated from either the barbed end of short 568-Alexa actin segments or mother filament bound Arp2/3 complex-VCA, forming mother or daughter filaments, respectively. This mixture was pipetted into flow chambers where the short, red actin segments bind the neutravidin coated coverslip surface and the branching reaction was allowed to continue for 1-2 min. The total time of branch formation and aging for a given experiment (e.g. 2.6 min) is indicated in the text. Branch formation and filament elongation was then terminated by removing untethered proteins (labeled actin, Arp2/3 complex and GST-VCA) from the sample chamber with gentle flow of KMIE buffer. Tethered filaments were further aged for different time periods after the removal of unbound protein. Low (2 μL min^{-1}) flow applied during aging ensured irreversible debranching. Filament segments with 568-Alexa-actin subunits (red; Fig. 1A) were tethered to the surface, while 647-Alexa actin (green; Fig. 1A) mother and daughter filaments were allowed to freely fluctuate and align with flow. Unlabeled actin monomer (0.2 μM) was included in flow buffer solution to prevent filament depolymerization. The "aging time" specified in each experiment is the time between the initial mixing of the proteins and application of debranching flow, including the time for branch formation and further aging. Debranching under force was performed by applying flow at a fixed rate (specified in text) throughout the experiment. Since unbound proteins were removed after the branch formation period, actin filament elongation was terminated, and

individual branch length (*l*) and consequently applied force (*F*) on the branch joint were constant (Eq. 5).

Experiments with BeF_x were performed two different ways. (a) For experiments with ATP-Arp2/3 complex (Fig. 3C inset), branches were formed from ATP-actin monomers and ATP-Arp2/3 complex as described above but with 2 mM $BeSO_4$ and 10 mM NaF included in the buffer at all times, and aged for 4 min before applying various rates of flow with KMIE buffer supplemented with 2 mM $BeSO_4$ and 10 mM NaF. For the experiment with BeF_x and 30 min aging (Fig. 3B, gray), ATP-Arp2/3 complex branches were formed as described above and aged for 30 min with 2 mM $BeSO_4$ and 10 mM NaF before applying flow with KMIE buffer. (b) For experiments with ADP-Arp2/3 complex and BeF_x (Fig 3B, brown), mother filaments with ATP-actin (10% biotinylated) monomers were immobilized on the surface as described above and the KMIE buffer (which includes ATP) was washed out and replaced with KMIE ADP buffer supplemented with 2 mM $BeSO_4$ and 10 mM NaF. Then ADP-actin monomers, ADP-Arp2/3 complex, and GST-VCA in KMIE buffer with 2 mM $BeSO_4$ and 10 mM NaF and 2 mM ADP instead of 2 mM ATP were gently flowed into the chamber and allowed to form branches. After a 4 min branch formation period, all unbound proteins were washed out with KMIE ADP and 2 mM $BeSO_4$ and 10 mM NaF and maintained under flow as noted. ADP-actin and ADP-Arp2/3 complex were prepared by exchanging nucleotide from ATP-actin and ATP-Arp2/3 complex, respectively, using desalting columns. ADP-Arp2/3 complex never formed branches unless 2 mM $BeSO_4$ and 10 mM NaF was present as reported previously and shown here (Fig. 5) (17, 24).

For experiments with AMPPNP mother filaments, filaments were polymerized from AMPPNP-actin monomers and immobilized on the surface as described above. Branch formation was initiated with ATP-Arp2/3 complex as described above in KMIE buffer with 0.2 mM AMPNP instead of 0.2 mM ATP. Since AMPPNP-Arp2/3 complex does not form branches (17), verified in my experiments (Fig. 5), all branches formed from Arp2/3 complex with bound ATP. Since the flow buffer included 0.2 mM AMPPNP, all actin monomers remained bound to AMPNP. The solution with Arp2/3 complex accounted for less than 1% of the final solution volume, so it introduced a negligible amount of ATP.

In debranching experiments with GMF with or without BeF_x, samples were prepared as above except that debranching was initiated by gentle flow of buffer (15 μL min^{-1}, very low force) containing a range of concentrations of GMF and the flow was maintained throughout the experiment.

Data analysis.

Analysis of branch dissociation was done by manual tracking with ImageJ (imagej.nih.gov). Branches that were fluctuating at all times and did not stick to the glass surface were selected randomly to minimize bias. These branches were labeled, catalogued and observed for their entire lifetimes. Origin (www.originlab.com) was used to fit all data and make plots. For the Arp2/3 complex debranching images in Fig. 1, a Gaussian blur with a sigma radius of 1.25 pixels was applied. Then images were background subtracted with a rolling ball radius of 15 pixels and subsequently contrast enhanced.

Chapter 3 – Arp2/3 complex stiffness cation binding site

I completed all work in this chapter and I received significant training, advice, and guidance from multiple people and labs while completing the work. I learned how to use the CRISPR/Cas9 system and handle *S. pombe* from the Berro Lab members Dr. Ronan Fernandez and Dr. Neal Ravindra. I learned how to perform negative stain electron microscopy from Dr. Mark Moosekar and Dr. Kaifeng Zhou. I learned how to perform the magnetic bead assay from Dr. Cesar Valencia, Dr. Olivia du Roure, and Dr. Julien Heuvingh. I am greatly indebted to those who shared their knowledge and expertise with me. I am truly grateful for their efforts and for spending their time to help me.

3.1 Abstract

The branched actin network generates and sustains the mechanical force required for cellular functions like cell motility and endocytosis. The network relies on mechanical properties such as stiffness to exert force on and resist force from the cell membrane. The main components of the network that give rise to the mechanical properties are actin, Arp2/3 complex, and cross-linking proteins such as fimbrin. Cations bound to a discrete cation binding site at the interface of neighboring actin subunits stiffen the actin filament and provide one method of control over actin mechanical properties. The cation binding sites in actin filaments are conserved in the Arp2/3 complex leading to the hypothesis that the Arp2/3 complex branch stiffness can be modulated by a cation binding site. To test this hypothesis, I disrupted the cation binding site to abrogate the ability of the Arp2/3 complex to bind to cations and compared the biochemical and biophysical properties of the mutant Arp2/3 complex to wild type (WT) Arp2/3 complex. I found that the mutations of the cation binding site residues have no effect on the growth, stiffness of Arp2/3 complex branches, or debranching under force. However, nucleation activity of the mutant Arp2/3 complex is slightly lower than the WT Arp2/3 and the Young's modulus of branched actin networks formed with the mutant Arp2/3 complex is ~25% lower than networks formed with WT Arp2/3 complex. The decreased Young's modulus could be due to fewer branches in the mutant networks or lowered branch stiffness of the mutant Arp2/3 complex. Further studies that precisely measure the number of branches in the network are required to interpret the reduced Young's modulus of networks formed with mutant Arp2/3 complex.

3.2 Chapter Introduction

The mechanical properties of actin filaments has been linked to discrete cation binding sites along the filament. The proposed cation binding site located at the interface of mammalian actin subunits is hypothesized to modulate the mechanics of the actin filament. Multiple amino acids comprise the cation binding site but the primary amino acid that contributes to the proposed cation binding site is Glutamate 167 (75). Glu167 is located directly at the surface of subdomain 3 and stabilizes cations via the D-loop of neighboring subunits. The proposed cation binding site has been engineered into actin from other species which lack the proposed cation binding site rendering the mechanical properties of the actin filament sensitive to cations (28, 75). For example, *S. cerevisiae* actin does not have a cation binding site because alanine is located at position 167. However, the mutation Ala167Glu confers a stiffness cation binding site into actin that can modulate the mechanical properties of the *S. cerevisiae* actin filaments.

Kang *et al* demonstrated that the mutation Ala167Glu into *S. cerevisiae* actin filaments renders the mechanical properties of the filaments sensitive to cations in solution (28, 75). WT *S. cerevisiae* actin filaments have a persistence length of ~2um and the persistence length does not increase as a function of $MgCl_2$. On the other hand, the persistence of *S. cerevisiae* actin filaments with the Ala167Glu mutation respond to $MgCl_2$. This was an interesting observation because the persistence length of most polymers decreases with increasing salt concentration due to charge shielding effects (76). The fact that additional salt increase persistence length suggested that the increased persistence length is due to increase subunit contacts due primarily to discrete cation binding.

The amino acids that comprise the proposed stiffness cation binding site in mammalian actin are conserved in mammalian Arp2 and Arp3 and are hypothesized to modulate the stiffness of the Arp2/3 complex branch junction via binding to a cation (28). It would be ideal to make mutations in the human Arp2/3 complex proposed cation binding site and measure the effect of the mutation. However, it is challenging to make mutations into the human Arp2/3 and purify it from recombinant systems (bacteria) like other small globular proteins because Arp2/3 complex is a 7-subunit complex. Therefore, I chose *S. pombe* as a model organism because the sequence of the Arp2/3 complex is very similar to human and the critical residues for cation binding are conserved (Fig. 1). I disrupted the proposed cation binding site of *S. pombe* Arp2/3 complex via site directed mutagenesis. I hypothesized that branches formed with the mutant Arp2/3 complex would be more flexible and be more complaint under force. I purified the mutant Arp2/3 complex and tested the hypothesis that the cation binding site modulates the stiffness of the Arp2/3 complex branch.

3.3 Results

The stiffness cation site found in actin is conserved in the Arp2/3 complex

Based on the engineered stiffness cation binding site in *S. cerevisiae* actin, the De La Cruz lab proposed the hypothesis that the Arp2/3 complex also contains a similar stiffness cation binding site due to the conserved sequence and this cation binding site may control the stiffness of the branch junction (28). To test this hypothesis, I used the Clustered Regularly Interspaced Short Palindromic Repeats (CRISPR) Cas9 system in collaboration with the Berro Lab to engineer the following mutation Arp2 Glu167Ala and Arp3 Glu198Ala in *S. pombe* Arp2/3 complex Fig 1. The Arp2 E167A Arp3 E198A mutations were designed based on the conserved sequence and on structural similarities to the action binding site of actin. I measured the growth of the Arp2/3 complex mutant E167A Arp2 E198A Arp3 mutants under stress conditions which included chemical and temperature stress and observed no major growth defects, suggesting that the original amino acids are not extremely important for biological function, Fig 2. This data cannot rule out that the engineered mutations reduced the activity or function of Arp2/3 complex and other compensatory mechanics such as mutations or regulation of protein levels compensated for the effects of a defective Arp2/3 complex. Lastly, although no observable growth defects were measured, CRISPR can cause off target mutations and future people who use this train should consider this for their particular applications.

The Arp2/3 complex branch angle or force-sensitivity to debranching was unaffected by the mutations E167A Arp2 E198A Arp3

I used electron microscopy of negatively stained samples to measure the branch angle of Arp2/3 complex branches formed with WT or mutant Arp2/3 complex and observed no

difference in the mean or standard deviation of the branch angle. Briefly, branches were formed by mixing 3 µM G Actin, 180 nM Arp2/3 complex and 0.5 µM GST-VCA and incubated for 2-3 minutes. Branches were immobilized on grids with 1% uranyl acetate, details in methods. At least 50 branches were selected for both WT and mutant Arp2/3 complex and the angle of each branch was measured by hand using Image J angle selection tool. A typical Arp2/3 complex branch is shown in Fig 5. The mean branch angle was 72.1 ± 1.72° for WT Arp2/3 complex and 73.7 ± 1.56° mutant Arp2/3 complex, indicating that there is very little or no observable difference in the mean and standard deviation of the branch angles, Fig 3A.

I measured the dissociation of Arp2/3 complex branches formed with WT and mutant Arp2/3 complex branches while applying 500 µL min^{-1} of buffer flow and found that there was no observable difference in rates of dissociation under force. I assembled branches and immobilized them on the glass surface as described in Chapter 2. I aged the branches for 4 minutes to capture both "young/strong" and "old/weak" mechanical states of the Arp2/3 complex and then applied constant buffer flow with a rate of 500 µL min^{-1}. I recorded branch dissociation by hand with Image J and plotted the fraction of branches remaining as a function of time to obtain time courses of debranching, Fig 3D. Both traces fit well to a double exponential with rate constants of WT fast phase lifetime of 0.2 ±0.01 min and slow phase 3.5 ±0.1 min and mutant fast phase lifetime of 0.2 ±0.03 min and slow phase 2.0 ±0.07 min. Both the fast phase and slow phase dissociation rate constants and their relative amplitudes of both WT and mutant Arp2/3 complex are similar, suggesting that the dissociation rate constant of both weak and strong states of the Arp2/3 complex of WT and mutant are similar. Additionally, since both WT and

mutant Arp2/3 have similar amplitudes at the same age time, the hydrolysis of bound ATP is probably not vastly different in the mutant Arp2/3 complex compared to WT Arp2/3 complex.

The mutations E167A Arp2 E198A Arp3 into the Arp2/3 complex slightly reduced nucleation activity

I used TIRF microscopy to measure the nucleation activity of WT Arp2/3 complex and mutant Arp2/3 complex and found that the mutant Arp2/3 complex was slightly defective in nucleation. Aged 10% biotinylated 488 Alexa-actin filaments were bound to the surface of a glass chamber via biotin-neutravadin interaction. Subsequently, 600 nM 15% 647-G Actin, 30 nM Arp2/3 complex, and 500 mM GST-VCA in 1x KMIE buffer was pipetted into the chamber and branch formation was observed immediately. The formation of branches and total length of mother filaments in the field of view was used to calculate the number of branches per mother filament length, Fig 3B. In future experiments, a wide concentration range of Arp2/3 complex and actin should be tested because the concentrations, specifically of lower concentrations of actin, could reveal greater nucleation defects. Additionally, a model to quantify the nucleation rate constants should be used. Because of time limitations and focus on other projects, I did not complete a concentration range and did not develop a model to quantify this data. Therefore, I cannot quantitatively assign the difference in nucleation activity of WT or mutant Arp2/3 complex for data from the TIRF.

I used pyrene fluorescence to compare the nucleation activity of WT Arp2/3 complex and mutant Arp2/3 complex and found that the mutant Arp2/3 complex was slightly defective in nucleation. I used 3 µM actin monomers (30% pyrene labeled), 200

nM Arp2/3 complex, and 500 nM GST-VCA at 25 °C. All proteins were mixed immediately before recording and fluorescence emission was recorded with 407 nm (excitation wavelength = 365 nm) in a plate reader. I calculated the concentration of barbed ends at half maximal polymerization and founded that the concentrations were 21 nM for WT and 14 nM for mutant Arp2/3 complex suggesting that the mutant Arp2/3 complex produces less branches since the concentration of barbed ends is lower than WT Arp2/3 complex.

The Young's modulus of branched actin networks formed with E167A/E198A Arp2/3 complex is lower than networks formed with WT Arp2/3 complex

I used a magnetic bead compression assay to measure the Young's modulus of branched actin networks formed with WT or mutant Arp2/3 complex and found that the Young's modulus of networks formed with mutant Arp2/3 complex is ~25% lower than networks formed with WT Arp2/3 complex. I performed these experiments under the guidance of Olivia du Roure and Julien Heuvingh at the ESPCI in Paris. Branched actin networks were formed by mixing 4.5 µM 5% 488 Alexa labeled actin monomers, 16.65 µM profilin, 100-400 nM *S. pombe* Arp2/3 complex, 90 nM capping protein, and beads coated with pWa. This mixture was immediately pipetted into a flow chamber constructed with double sided tape and sealed with wax. After approximately 5-10 min branched actin networks formed with WT Arp2/3 complex grew to approximately 200nm larger than the dyna bead and networks formed with mutant Arp2/3 complex grew to similar a size after approximately 10-15 min. This difference in rate of network formation could be due nucleation defects in the mutant Arp2/3 complex. The difference in Young's modulus could be due to a differences in mechanical properties of the Arp2/3 complex or

due to a difference in the number of branches, as shown by previous experiments (77). To definitively understand the difference in Young's modulus formed by mutant and WT Arp2/3 complex branched networks, the nucleation activities of both Arp2/3 complexes must be measured precisely and more importantly, the effect of nucleation of the number of branches in the networks must be measured.

3.5 Figures

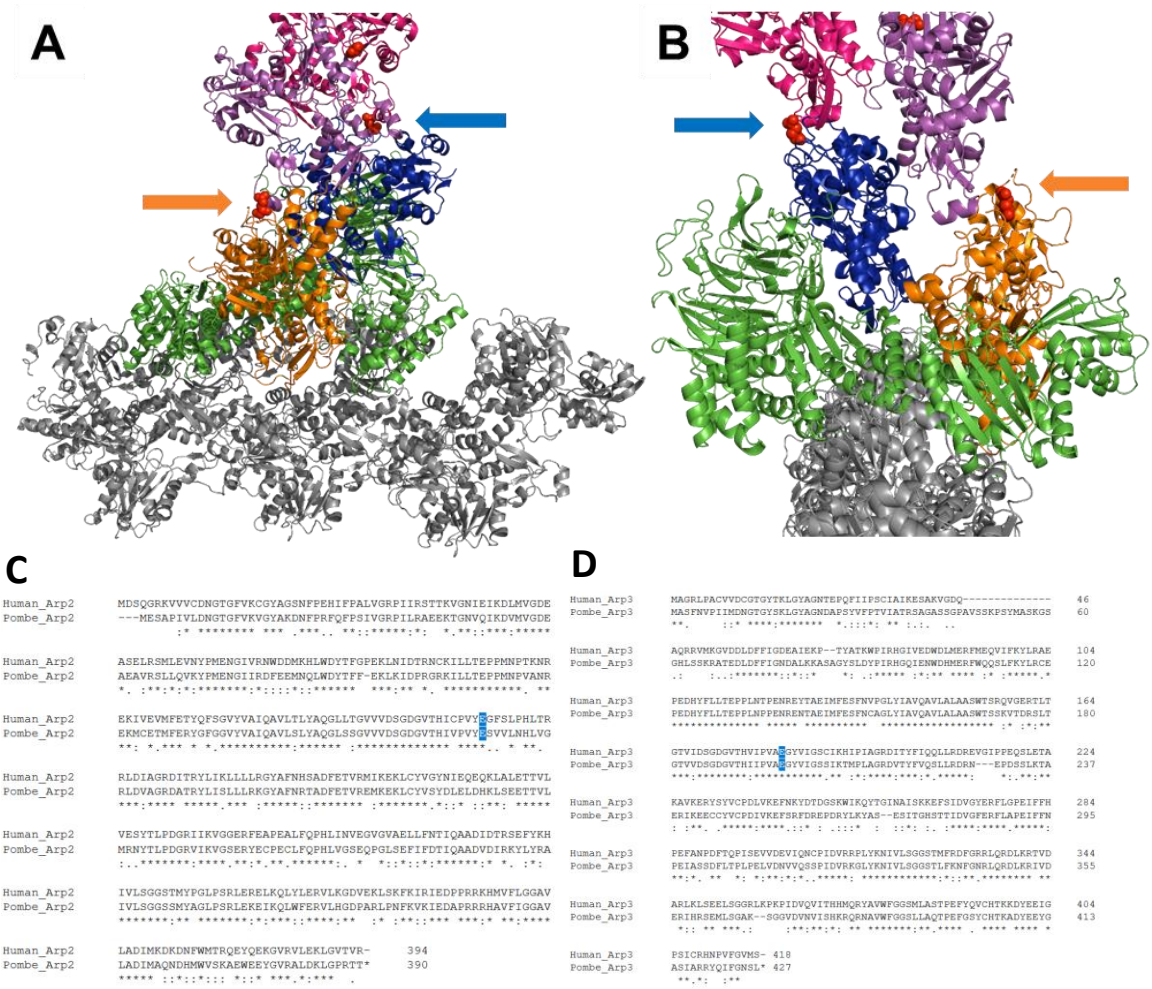

Figure 1. Proposed cation binding sites in the Arp2/3 complex.

A molecular representation of the Arp2/3 complex bound to a mother filament via an unpublished protein coordinate file obtained directly from professor Thomas Pollard. Panel A (side view) and B (long-axis of an actin filament) are identical except B is rotated 90°. The mother filament is represented in gray. The Arp2 and Arp3 subunits are represented in blue and orange respectively. The remaining 5 subunits of the Arp2/3 complex are in green. The first two actin subunits of the daughter filament are in different shades of pink. Mutations that disrupt the proposed cation binding site are represented as

red spheres. Arrows point to the location of the proposed cation binding sites that are located at the interface between the Arp2 (blue) and Arp3 (orange) subunits and daughter filament actin subunits. (C &D) Sequence alignment comparison from Clustal Omega of Arp2 and Arp3 proteins from human compared to *S. pombe*.

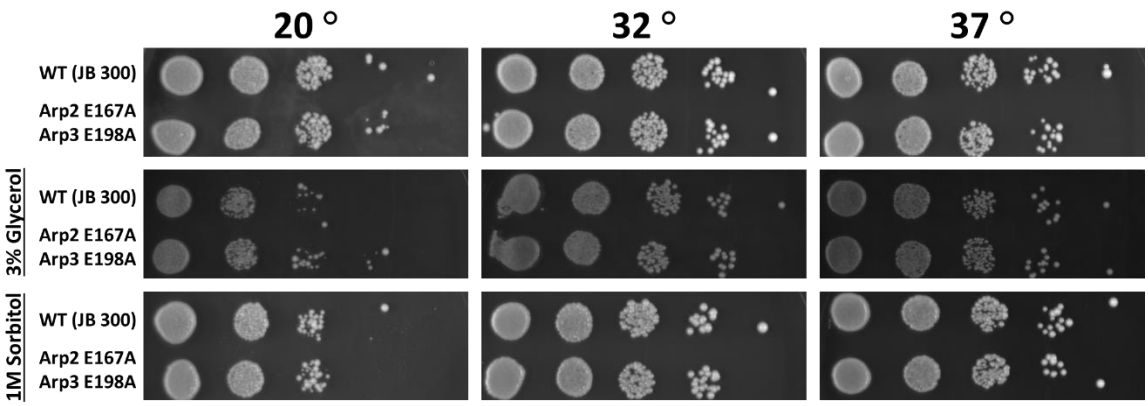

Figure 2. The effect of Arp2/3 proposed cation binding site mutations on growth of *S. pombe*

The E167A/E198A mutation into the Arp2/3 complex does not cause major growth defects under stressful conditions compared to WT Arp2/3 complex in *S. pombe*. *S. pombe* was grown using standard YE5S media to 0.4 OD and diluted by 10,100,1000, or 10000 fold and plated onto YE5S plates with 1M sorbitol or 3% glycerol, and grown for 2-3 days at 20, 32, or 37 C°. The growth of each strain after 2-3 days on each plate under different conditions was recorded using a camera.

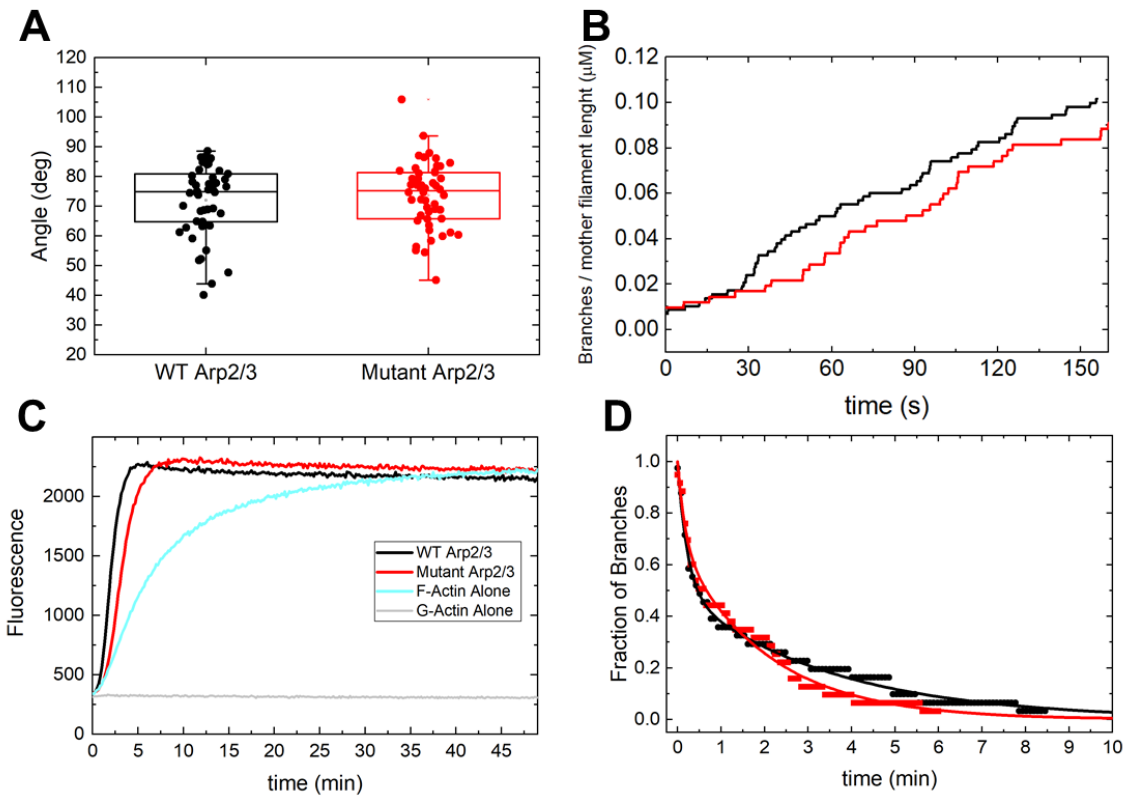

Figure 3. The effect of E167A/E198A mutations on Arp2/3 complex on branch angle, nucleation, and debranching activities.

All black symbols and curves correspond to WT Arp2/3 complex and red curves correspond to E167A/E198A Arp2/3 complex. All experimental details are reported in the methods section while some important conditions are provided here for ease. (A) Comparison of branch angle of WT and E167A/E198A Arp2/3 complex as measured by electron microscopy of negatively stained samples and plotted with a box and whiskers plot. For WT Arp2/3 complex the mean is 72.1 ± 1.72° and for E167A/E198A Arp2/3 complex 73.7 ± 1.56°. The buffer used here is 1x KMIE. Branch angles were measured by hand in ImageJ, details in methods. (B) The number of branches formed s^{-1} per mother filament length as directly observed by TIRF microscopy. Filaments with 10% biotinylated 488-Alexa actin monomers were bound to the surface of the glass. KMIE

buffer with 600 nM 647-G Actin, 30 nM Arp2/3, and 500 mM GST-VCA was pipetted into the chamber. Immediately after, branch formation and length of mother filament's bound in that field were recorded over time and counted with ImageJ. The plot shows the number of branches per second divided by the total length of the mother filament which remains constant over time. Only branches grown on the original mother filament are counted and not branches growing from new branches. (C) Comparison of nucleation activity of WT and E167A/E198A Arp2/3 complex by the time course of pyrenal-actin polymerization. Conditions: 1x KMIE buffer. Black and red trace: 3 µM actin monomers (30% pyrene labeled), 200 nM Arp2/3 complex, and 500 nM GST-VCA at 25 °C. Blue trace: 3 µM actin monomers (30% pyrene labeled). All proteins were mixed immediately before recording and fluorescence emission was recorded with 407 nm (excitation wavelength = 365 nm) in a plate reader (Molecular Devices, SpectraMax GEMINI XPS). At half max polymerization the concentration of free barbed ends was 21 nM for WT and 14 nM for Mutant Arp2/3 complexes. (D) Comparison of WT and E167A/E198A Arp2/3 complex debranching with 500 ul/min buffer flow rate corresponding to approximately ~1 pN of force for a branch with length 1um. Branches were formed and dissociation under force was measured as described in Chapter 2. Smooth curves are the best fits of double exponential decays with lifetimes yielding WT - fast phase lifetime of 0.22 ±0.01 min and slow phase 3.47 ±0.09 min and Mutant - fast phase lifetime of 0.17 ±0.03 min and slow phase 2.03 ±0.07 min.

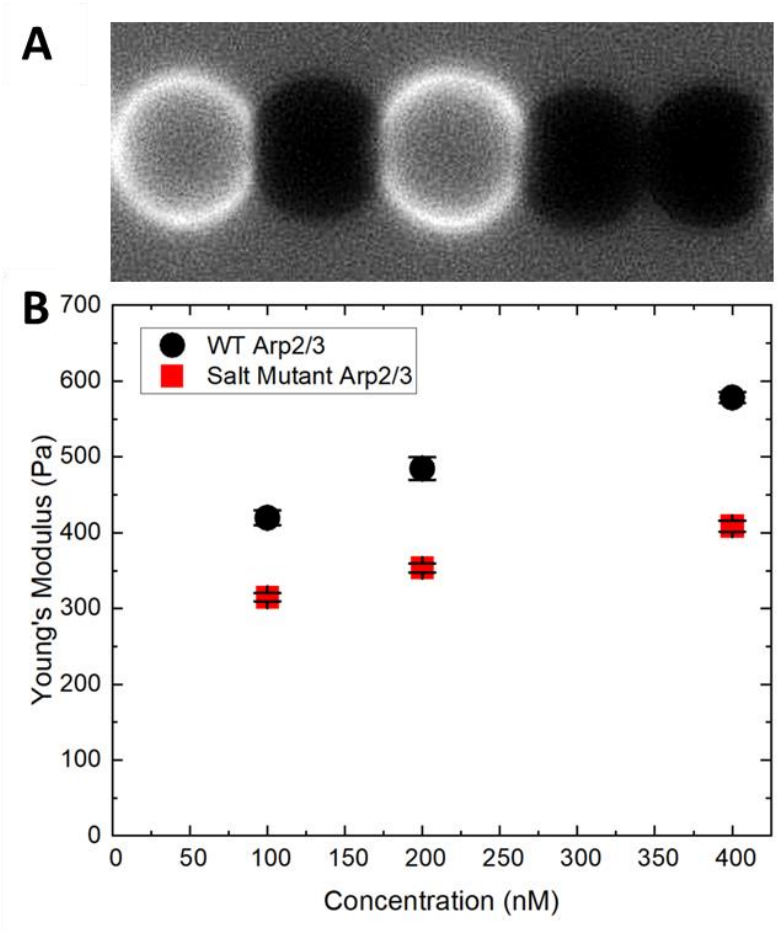
A
B
WT Arp2/3
Salt Mutant Arp2/3
Young's Modulus (Pa)
Concentration (nM)
0
100
200
300
400
500
600
700
0
50
100
150
200
250
300
350
400

Figure 4. Branched actin networks formed with the mutant Arp2/3 complex have a lower Young's Modulus compared to WT Arp2/3 complex

All experimental details are reported in the methods section while some important conditions are provided here. (A) A representative image of the magnetic bead compression assay. 4.5 µm Dyna 450 epoxy beads are coated with pWa or BSA. These beads are mixed with 4.5 µM 5% 488 Alexa G-Actin, 100-400 nM (WT or Mutant) Arp2/3 complex, 16.65 µM profilin, 90 nM capping protein in 1x KMIE. Beads coated with pWa grow branched actin networks around them and a bright "gel" is observed whereas the dark beads are coated only with BSA and remain dark. After the radius of the network is at least 200 nm larger than the bead, a gradually increasing magnetic field is applied and then gradually released while the centroid of the bead is tracked with nanometer precision to calculate the deformation of branched actin network. Young's modulus is calculated as described in (77) and described in detail in methods. A stiffer branched actin network deforms less compared to a softer one and will have a lower Young's modulus. (B) Comparison of the Young's modulus of branched actin networks formed with various concentrations of WT (black circles) Arp2/3 complex or mutant Arp2/3 (red squares) Arp2/3 complex after at least 3 minutes after of network assembly is completed. Each data point represents a mean of more than 100 measurements recorded on 3 different days. Error bars represent the SEM of the entire data set with $n > 300$ for each measurement (across all days).

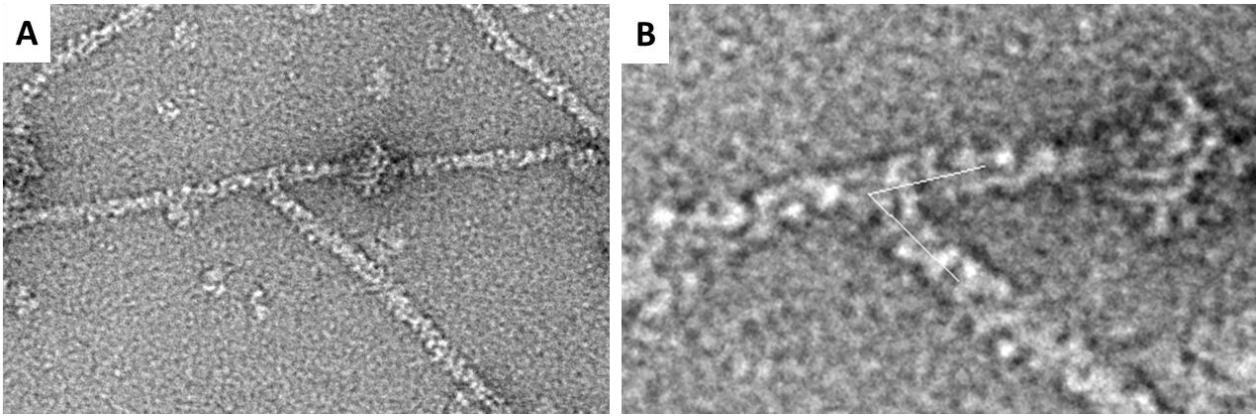

Figure 5. Electron microscopy of negatively stained Arp2/3 complex branches

A typical negative stained Arp2/3 complex branch. All experimental details related to sample preparation are reported in the methods section. (A) A cropped image from a micrograph at 73000x zoomed in for clarity. (B) An example of measuring the Arp2/3 complex branch using the Image J "Angle Measurement Tool". This particular branch had an angle of 60 degrees.

3.4 Discussion

I tested the hypothesis that the Arp2/3 complex contains a cation binding site that modulates the stiffness of the junction by binding to cations. I made a mutation of the proposed cation binding sites of the Arp2 and Arp3 subunits of the Arp2/3 complex (E167A-Arp2 E198A-Arp3) because these mutations are expected to disrupt the proposed cation binding site. I compared the biochemical and biophysical properties of the mutant to the WT Arp2/3 complex and the data I collected shows that there are no observable differences between the WT and mutant Arp2/3 complexes in bulk growth assays in stress conditions, branch angle, or debranching under force. However, the mutant Arp2/3 complex is slightly lower in nucleation activity and may explain the lower Young's modulus of the networks formed by mutant Arp2/3 complex. Alternatively, the reduced Young's modulus could be because the mutant Arp2/3 complex is more compliant under load compared to WT Arp2/3 complex. However, this conclusion is impossible to confirm until the number of branches in the branched actin network is quantified because the Young's modulus depends on the number of branches.

Reasoning for Arp2/3 complex mutations and effect on growth

The hypothesis that cations modulate the stiffness of the Arp2/3 complex branch junctions originated from a structural comparison of actin and Arp2/3 complex (28). Based on this structural comparison, I made the mutations (E167A-Arp2 E198A-Arp3) because these mutations are expected to disrupt the cation binding site and consequently abrogate the ability of the Arp2/3 complex to bind cations. Although the proteins Arp2 and Arp3 are very similar to actin in sequence and structurally, the Arp2/3 complex may not rely on cation binding for junction stiffness and may rely on factors such as numerous

protein-protein interfaces. The mutations have no observable growth defects even under stress, suggesting that they are not critical for function or the organism complemented the mutation in some unknown way. To determine if compensatory mechanisms occurred in the mutant strain, it is possible to sequence the genome to see if other mutations were present or it is possible to check if the concentrations of other proteins were altered, specifically during functions like endocytosis. A full genome sequencing of the mutants could reveal any compensatory mutations. To determine if the concentration of other proteins was altered during endocytosis, the number of molecules during endocytosis could be measured via quantitative fluorescence microscopy. It is possible that the mutations could result in a softer network resulting in the need for increased actin or cross-linking proteins such as fimbrin to stiffen the network and generate the required force to deform the membrane. A quantitative western blot to measure concentrations of a proteins that are likely to be affected (actin, fimbrin, capping protein, etc) is also possible.

Effects of mutations in the Arp2/3 complex on branch angle and debranching

There are multiple possibilities that could explain why the mutations had no observable effect on the branch angle. First, the effect of the mutations could simply not be important for the stiffness of the branch angle if the branch angle stiffness relies on other structural properties of the Arp2/3 complex. For example, the Arp2/3 complex contains 7 subunits, three that interact with the mother filament and two that interact with the daughter filament. The mutations I made are on the interface of the subunits (Arp2 and Arp3) which interact with the daughter filament. If the stiffness of the branch angle is modulated primarily by the mother filament interface, then the mutations would have no effect on branch stiffness. Alternatively, the 2 mutated amino acids comprise only a small

fraction of the total interface area between the Arp2/3 complex and the mother filament. So, the mutations may have a small effect on the structure/stiffness of the entire complex compared which spans over a much larger area.

Second, the method to measure branch angle stiffness (negative stain EM) relies entirely on accurately capturing the fluctuations of the branch angle and may not be sensitive enough to observe any changes in branch angle stiffness. The branch angle could be different due to the mutations, but if the difference is ~<3°, then even negative stain electron microscopy may not be able to capture this difference accurately. Furthermore, the first ~50-100 nm of the branch, which include ~18-36 actin subunits, are used to measure the branch angle. If the change in the angle is only between the Arp2/3 complex and the first subunit of the daughter filament, a much high resolution is required to observe a change and measuring the first ~18-36 subunits would mask any change in angle.

Lastly, there may be other amino acids important for the cation binding site in the Arp2/3 complex other than the Glu167 which are not important in actin. New potential mutations predicted via more detailed structural bioinformatics analysis could be tested in the future. It is also possible that there may be no cation binding site in the Arp2/3 complex even though it is clearly present in actin. The *S. pombe* Arp2/3 complex may not have a detectable cation binding site but Arp2/3 complexes from other organisms may have one and could be important for mechanics.

Effects of mutations in the Arp2/3 complex on nucleation and debranching

The mutant Arp2/3 complex has decreased nucleation activity as measured directly by TIRF microscopy and by bulk pyrene fluorescence but these measurements provide little or no mechanistic explanation. Below I discuss a few possibilities that may contribute to the decreased nucleation activity.

Since the mutations are at the interface of the Arp2/3 complex and incoming monomer, the reduced nucleation activity could be due to decreased affinity of the incoming actin monomers prior to branch formation. Before branch formation, the Arp2/3 complex is bound by two activating proteins (in this work, one single dimeric activator GST-VCA) which are thought to shuttle in one or both actin monomers (18, 19) preceding branch elongation. Subsequently, the activator dissociates (18, 55) and branch elongation begins. If the new actin monomers interacting with the mutated Arp2/3 complex dissociate faster than compared to WT Arp2/3 complex before branch formation can occur, it could result in decreased nucleation activity. It is unlikely that the affinity for the mutant Arp2/3 complex and daughter filament is different compared to WT Arp2/3 and daughter filament in a mature branch because branches formed from both complexes have similar dissociation rate constants under ~1 pN of force. So, the affinities for the actin monomers could be different before and after branch formation. However, the WT Arp2/3 complex dissociates with the daughter filament during a debranching event which shows that that the weakest interface is probably between the Arp2/3 complex and the mother filament. Therefore, it is not surprising that the mutated interface does not affect debranching. It is important to note that it is unknown if the mutant

Arp2/3 dissociates with the daughter or remains bound to the mother because it was never labeled and observed during debranching.

There are a few other possible explanations for the reduced nucleation activity. For example, decreased affinity to mother filament before branch formation, decreased affinity for ATP which is required for branch formation, or decreased affinity for activator. Less than 1% of Arp2/3 complex binding events to the mother filament result in branch formation (19). If the dissociation rate constant (prior to branch formation) of the Arp2/3 complex from the mother filament is increased, it could also result in an observed nucleation activity because less branches would form. Since ATP bound to the Arp2/3 complex is a prerequisite for branch formation, if the mutated Arp2/3 has a decrease affinity for ATP, this could affect observed branch formation (17). It is possible that the affinity of the mutant for the activator GST-VCA could be reduced. However, since there is a large excess of GST-VCA bound on the column during purification, any modest difference in affinity would not be observed.

Mechanical properties or nucleation defects can lead to decrease Young's modulus

Branched actin networks formed with mutant Arp2/3 complex have a ~25% decreased Young's modulus compared to WT Arp2/3 complex at all concentrations tested and there are multiple explanations for this observation. First, it is possible that the mutant Arp2/3 complex is more complaint when under load even though the branch angle stiffness without load is undistinguishable from WT Arp2/3 complex. It is possible that the cumulative effect of many slightly weaker branches in a network with presumably hundreds of branched actin filaments could easily result in a decreased Young's modulus of the entire network. Alternatively, the reduced nucleation activity of the mutant Arp2/3

complex could result in fewer branches in the network and could also explain the decreased Young's modulus because the Young's modulus is affected by the number of branches. Since the number of Arp2/3 complex branches in the dense branched actin network could not observed, it is unfortunately impossible to differentiate between the two possibilities. I attempted to count the number of branches with labeled WT Arp2/3 complex in the network but since the network density is so high, it was impossible to distinguish individual branches and count them. It may be possible with a small ratio of labeled to unlabeled Arp2/3 complex branches, but unfortunately completing this experiment is only possible in Paris, France in the du Roure lab due to their equipment and expertise.

3.5 Methods

Growth Assays

S. pombe, WT (JB 300) and JB300 with the mutations Arp2 E167A and Arp3 E198A, were grown in YE5S at 32° to OD 0.4. Cultures were diluted 10,100, 1000, or 10,000 fold and plated onto YE5S media plates supplemented with 3% glycerol or 1M Sorbitol and grown for 2-3 days at 20, 32, or 37 C°.

Negative stain electron microscopy

Branched actin networks were assembled with 200 nM Arp2/3 complex, 500 nM GST-VCA, and 3 μM rabbit skeletal actin Mg-actin monomers in 1x KMIE buffer (50 mM KCl, 2 mM $MgCl_2$, 10 mM Imidazole, 1 mM EGTA, 0.2 mM ATP, 2 mM DTT) for 2-3 minutes. This solution was diluted 10-20 fold and pipetted onto a copper mesh grid (FCF300-CU from Electron Microscopy Sciences) and coated with 1% uranyl acetate. Excess solution was wicked of gently with a paper towel and allowed to dry in the fume hood for 5-10 min. Images were taken on a FEI Talos L120C in Bass Center, Yale University with 40,000x to 90,000x magnification. A typical Arp2/3 complex branch image can be seen in Fig. 5.

TIRF microscopy to measure nucleation activity of Arp2/3 complex

Microfluidics chambers were constructed as described previously in methods section of Chapter 2 and used in these experiments here. Actin filaments were assembled with 10% biotin and 15% 488-Alexa ATP-Mg bound actin monomers with 1x KMIE at room temperature for 1 hour. These filaments were pipetted into the microfluidic chamber and immobilized on the surface via biotin-neutravadin interaction. Unbound filaments were

washed away with 1x KMIE. Next, 600 nM 15% 647-G Actin, 30 nM Arp2/3 complex, and 500 mM GST-VCA in 1x KMIE buffer was pipetted into the chamber to allow for branch formation. Immediately after, video recording was started to capture branch formation with a 10 frames s^{-1} frame rate. After approximately 2-3 minutes, the field of view was too dense to observe new branch formation so the experiment was terminated. The time of branch formation and length of mother filaments were recorded by hand using ImageJ.

Pyrene actin polymerization assays

Actin monomers at concentration of 3 µM actin monomers containing 30% pyrene labeled monomers, 200 nM Arp2/3 complex, 500 nM GST-VCA were mixed together in 1x KMIE and polymer growth was observed immediately using a plate reader (Molecular Devices, SpectraMAX Gemini XPS) with 365 nm excitation light and 407 emitted light.

Debranching under force assays

Debranching under force assays were completed as described in section "Preparation of branched actin filament networks and experimental procedures" in Chapter 2.

Magnetic bead compression assay

Dyna 450 epoxy beads that were 4.5 µm in size were coated with GST-pWa (mammalian Arp2/3 complex activator) or BSA according to the manufacture's specification. Briefly, beads were washed three times with 20 mM Tris buffer with 50 mM KCl and then incubated with either 2 µM pWa or 1 mg/ml BSA. Finally, beads were washed with the same buffer supplemented with 0.1 % BSA. Equal quantities of GST-pWa coated and BSA coated beads are mixed with 4.5 µM 5% 488 Alexa G-Actin, 100-400 nM (WT or

Mutant) Arp2/3 complex, 16.65 µM profilin, 90 nM capping protein in 1x KMIE. Beads coated with pWa grow branched actin networks around them and a bright "gel" is observed whereas the dark beads are coated only with BSA and remain dark. This mixture is pipetted into a microfluidic chamber and sealed with wax so the concentration of proteins remains constant. Fluorescent branched actin networks (the bright beads) grow on the beads and are visible after 5-15 minutes. After the radius of the network is at least 200 nm larger than the bead, a gradually increasing magnetic field is applied and then gradually released. While applying and releasing the magnetic field, the centroid of the bead is tracked with nanometer precision to calculate the deformation of branched actin network. Measurements of the network are only taken at the interface of pWa-coated beads and BSA coated beads so the branched network is compressed with the hard (unyielding) surface of the BSA-coated. Force and Young's Modulus is calculated as described in (77). Briefly, force on the networks is calculated from the applied magnetic field (3-80 mT) and contact area of the bead using a Hertzian contact model. Young's modulus is calculated from the stress on the network (stress=force/area) and the observed deformation of the branched actin network (strain=change in length/length) where F is force, A is area, and l is length.

$$Young's\ Modulus = \frac{stress}{strain} = \frac{\frac{F}{A}}{\frac{\Delta l}{l}} \qquad \text{Eq.6}$$

Chapter 4 – Conclusions

In this section I highlight the 5 main conclusions of my work and discuss why I believe these conclusions are important for the field.

1 - Branches formed by Arp2/3 complex are very sensitive to force because small piconewton forces reduce the lifetime of Arp2/3 complex branches from hours to seconds. There is a significant discrepancy between the lifetime of branches *in vivo* and lifetimes measured *in vitro* (in experiments without regulatory proteins like cofilin/GMF); branches in the cell turn over much faster than *in vitro*. My finding that forces accelerates debranching could help explain this discrepancy suggesting that forces in the cell could allow for fast disassembly. One other explanation for this discrepancy could be that regulatory proteins that accelerate debranching found in cells are absent from the *in vitro* experiment. Since both forces and regulatory proteins are present in cells, I expect that both factors modulate Arp2/3 complex branch lifetimes in the cell and consequently both force and regulatory proteins may interact with one and other. So, this observation leads to new questions to about the interaction between force and regulatory proteins to modulate Arp2/3 complex lifetimes. Lastly, this new force-dependent debranching parameter can be included in models to improve predictions and descriptions of network turnover.

2 - Branches formed by Arp2/3 complex have two mechanical states with different force sensitivities. Phosphate release from Arp2/3 complex causes the transition from the strong to the weak state. Why the Arp2/3 complex is an ATPase is unknown and the reports on the ATPase activity have been contradictory. My work further differentiates the two main contradictory reports and favors a mechanism that phosphate release

accelerates debranching but does not trigger it. Since ADP branches are long lived in the absence of force (~hours), it eliminates the hypothesis from Carlier lab (16) that hydrolysis triggers branch formation.

Furthermore, the findings here may improve the quality of *in vitro* experiments for all other researchers. Most measurements of the Arp2/3 complex occur at anytime after branch formation and the age of branch lifetimes is not considered or reported and this may explain some of the discrepancies between labs such as binding affinities reported for GMF binding to Arp2/3 complex. However, this work clearly shows that there is a transition in both biochemical and biophysical properties that change over time (due to phosphate release) and so researchers may account for "age time" in the future for their experiments. This is analogous to how researchers must "age" actin filaments into the ADP actin state before making measurements with cofilin because cofilin interacts differently with ADP and ADP-P_i.

3 - Neither the force on the mother filament nor the nucleotide bound to the mother filament affect Arp2/3 complex branch lifetime. Interpretation of data from a previous report suggested that the mother filament nucleotide state affects the Arp2/3 complex branch lifetime and the work here may provide a new interpretation (39). Due to improved surface functionalization, the work here does not rely on surface bound myosin's to capture branches and therefore may overcome a limitation in previous experiments.

Since only the nucleotide state of the Arp2/3 complex controls the branch lifetimes, this regulatory mechanism provides an additional and independent "internal timer" (actin is another one) that will could be important for regulating network turnover.

Meaning, the nucleotide state of actin and Arp2/3 complex ould be controlled and targeted independently which allows for multiple levels of regulation. Lastly, this observation provides more evidence to support the dendritic nucleation hypothesis.

4 - The Arp2/3 complex and branch dissociate from the mother filament within 100 ms of each other. This is an important finding because it eliminates the possibility that the Arp2/3 complex cannot immediately form new branches at the location it was bound and so it must dissociate, re-bind ATP, re-bind the activator, and then form new branches. This places both physical and time constraints on the role of individual Arp2/3 complexes; branches can ONLY form at the leading edge since they will require a freshly ATP-bound Arp2/3 complex and a membrane bound activator and debranching within the older portions of the network cannot trigger new branch formation.

5 - GMF only dissociates “old” branches with bound ADP and the debranching activity is slow. This observation is again consistent with the dendritic nucleation hypothesis because it provides direct evidence for another analogous regulatory mechanism; GMF can specifically target older branches for turnover similar to how cofilin targets older filaments by turnover. Since GMF and cofilin are so homologous it is no surprise that they both rely on the nucleotide state of their targets for regulation and activity. Lastly, since GMF activity is relatively slow, it places an upper limit on how fast GMF may act and also suggests that GMF will not be able to act on newly formed branches. Since GMF affinity is very tight, many GMF molecules are not required for function in the cell. It would be interesting to investigate if there is a biological mechanism to accelerate GMF activity such as a binding protein to chaperone GMF to an Arp2/3 complex or PTMs on the GMF directly.

Chapter 5 – Future directions and speculations

During the course of my thesis research I have kept a note book of questions that have interested me and questions that came up during discussion with others, specifically Dr. Anthony Schramm, Dr. Wenxiang Cao, Dr. Jeff Bibeau, Shawn Gray, and Professor Enrique De La Cruz. Below, I highlight the most interesting (interesting to me at least) follow-up experiments that could be the topic of future investigations.

Arp2/3 complex follow-up experiments

It would be interesting to compare the branch angle of different Arp2/3 isoforms and use differences in their inherent structure to identify/predict which components may lead to differences in branch angle. A detailed bioinformatics or molecular dynamics study maybe able to predict the most important differences between the isoforms and side directed mutagenesis may be able to test those predictions.

The nucleotide state of the Arp2/3 complex may also affect the branch angle and branch stiffness since it clearly controls the biophysical properties such as sensitivity to force. So, it would be interesting to measure the branch angle of ADP and ADP-BeFx branches and check if there are any differences. I actually do expect a difference because the branch angle because it is critical for efficient force generation when the Arp2/3 complex is near the membrane but is less important as the Arp2/3 complex treadmills away form the membrane (when it is most likely in the ADP state). The change in branch angle could reflect a change in conformation (ADP-BeFx to ADP) and may recruit debranching proteins different (see below). This change in conformation could be very small, similar to how a change in flexibility of the D-loop in ADP-P_i actin reduces the affinity of cofilin to the actin filament (7). If the nucleotide does affect branch angle (or

branch angle variation), the branch angle could be use as an indicator for the nucleotide state of the Arp2/3 complex and this indicator would be useful studying Arp2/3 binding proteins. A Hidden Markov Model could be used to predict the probability the nucleotide state (hidden state) based on the branch angles (observed data).

GMF follow-up experiment

The data I collected revealed that GMF preferentially dissociates branches with ADP-Arp2/3 complex branches over ADP-BeFx but the data provided no mechanistic detail on why. So, it would be interesting to identify if GMF binding, activity, or both is reduced be ADP-BeFx Arp2/3 complex branches.

It would also be interesting to check if GMF binds preferentially to Arp2/3 complex branches at a particular angle. The reason for this is the conformation of the Arp2/3 complex itself may change as the entire branch fluctuates between ~60° and 80° and this conformational change may be alter affinity for GMF binding. If branches within the branched actin network have unique branch angles at the leading vs bottom edge of the branched actin network, the angle of the branch may allow for specific targeting. Other proteins are sensitive to small changes in angle, for example Arp2/3 complex itself preferentially binds different angles of the actin filament (prefers convex angles over concave angles).

Although the affinity of GMF for ADP-Arp2/3 complex is high ($K_{d,\,GMF}$) of 40 (± 10) nM, the GMF activity is surprisingly slow ($k_{GMF} = 1/\tau_{GMF}$) of 0.31 (± 0.05) min^{-1}. This suggests that only a few GMF molecules (<10-50nM) in the cell could debranch most of the network (given that GMF unbinds from the Arp2/3 complex after debranching and then can bind to another Arp2/3 complex) although it would be a slow process. So, in

future experiments it would be interesting to find a mechanism by which GMF activity could be accelerated (binding protein, PTMs, or force). With such a mechanism, the GMF could be always present near the network but relatively "inactive" due to the slow activity but then be "triggered" on when needed.

Cortactin follow-up experiments

A wide range of questions related to how cortactin stabilizes the Arp2/3 complex remain unanswered. I think the three most critical questions are as follows. 1) Are cortactin bound branches more resistant to force? 2) Does cortactin stabilize the Arp2/3 complex by reducing the rate of phosphate release and/or through a physical tethering mechanism? 3) Does cortactin change the branch angle of the Arp2/3 complex?

References

1. T. D. Pollard, Regulation of actin filament assembly by Arp2/3 complex and formins. *Annu Rev Biophys Biomol Struct* **36**, 451-477 (2007).
2. T. D. Pollard, What We Know and Do Not Know About Actin. *Handb Exp Pharmacol* **235**, 331-347 (2017).
3. F. B. Straub, G. Feuer, Adenosinetriphosphate. The functional group of actin. 1950. *Biochim Biophys Acta* **1000**, 180-195 (1989).
4. M. F. Carlier, D. Pantaloni, Direct evidence for ADP-Pi-F-actin as the major intermediate in ATP-actin polymerization. Rate of dissociation of Pi from actin filaments. *Biochemistry* **25**, 7789-7792 (1986).
5. C. Suarez *et al.*, Cofilin tunes the nucleotide state of actin filaments and severs at bare and decorated segment boundaries. *Curr Biol* **21**, 862-868 (2011).
6. T. Masaike, E. Muneyuki, H. Noji, K. Kinosita, Jr., M. Yoshida, F1-ATPase changes its conformations upon phosphate release. *J Biol Chem* **277**, 21643-21649 (2002).
7. S. Z. Chou, T. D. Pollard, Mechanism of actin polymerization revealed by cryo-EM structures of actin filaments with three different bound nucleotides. *Proc Natl Acad Sci U S A* **116**, 4265-4274 (2019).
8. R. D. Mullins, J. A. Heuser, T. D. Pollard, The interaction of Arp2/3 complex with actin: nucleation, high affinity pointed end capping, and formation of branching networks of filaments. *Proc Natl Acad Sci U S A* **95**, 6181-6186 (1998).
9. I. Rouiller *et al.*, The structural basis of actin filament branching by the Arp2/3 complex. *J Cell Biol* **180**, 887-895 (2008).
10. P. A. Janmey, C. A. McCulloch, Cell mechanics: integrating cell responses to mechanical stimuli. *Annu Rev Biomed Eng* **9**, 1-34 (2007).
11. T. M. Svitkina, A. A. Neyfakh, Jr., A. D. Bershadsky, Actin cytoskeleton of spread fibroblasts appears to assemble at the cell edges. *J Cell Sci* **82**, 235-248 (1986).
12. T. D. Pollard, G. G. Borisy, Cellular motility driven by assembly and disassembly of actin filaments. *Cell* **112**, 453-465 (2003).
13. S. Wiesner *et al.*, A biomimetic motility assay provides insight into the mechanism of actin-based motility. *J Cell Biol* **160**, 387-398 (2003).
14. D. Pantaloni, C. Le Clainche, M. F. Carlier, Mechanism of actin-based motility. *Science* **292**, 1502-1506 (2001).
15. M. J. Dayel, R. D. Mullins, Activation of Arp2/3 complex: addition of the first subunit of the new filament by a WASP protein triggers rapid ATP hydrolysis on Arp2. *PLoS Biol* **2**, E91 (2004).
16. C. Le Clainche, D. Pantaloni, M. F. Carlier, ATP hydrolysis on actin-related protein 2/3 complex causes debranching of dendritic actin arrays. *Proc Natl Acad Sci U S A* **100**, 6337-6342 (2003).
17. M. J. Dayel, E. A. Holleran, R. D. Mullins, Arp2/3 complex requires hydrolyzable ATP for nucleation of new actin filaments. *Proc Natl Acad Sci U S A* **98**, 14871-14876 (2001).
18. B. A. Smith *et al.*, Three-color single molecule imaging shows WASP detachment from Arp2/3 complex triggers actin filament branch formation. *Elife* **2**, e01008 (2013).
19. B. A. Smith, K. Daugherty-Clarke, B. L. Goode, J. Gelles, Pathway of actin filament branch formation by Arp2/3 complex revealed by single-molecule imaging. *Proc Natl Acad Sci U S A* **110**, 1285-1290 (2013).
20. R. Basu, F. Chang, Characterization of dip1p reveals a switch in Arp2/3-dependent actin assembly for fission yeast endocytosis. *Curr Biol* **21**, 905-916 (2011).

21. A. R. Wagner, Q. Luan, S. L. Liu, B. J. Nolen, Dip1 defines a class of Arp2/3 complex activators that function without preformed actin filaments. *Curr Biol* **23**, 1990-1998 (2013).
22. A. C. Martin, M. D. Welch, D. G. Drubin, Arp2/3 ATP hydrolysis-catalysed branch dissociation is critical for endocytic force generation. *Nat Cell Biol* **8**, 826-833 (2006).
23. C. Le Clainche, D. Didry, M. F. Carlier, D. Pantaloni, Activation of Arp2/3 complex by Wiskott-Aldrich Syndrome protein is linked to enhanced binding of ATP to Arp2. *J Biol Chem* **276**, 46689-46692 (2001).
24. L. Blanchoin, T. D. Pollard, R. D. Mullins, Interactions of ADF/cofilin, Arp2/3 complex, capping protein and profilin in remodeling of branched actin filament networks. *Curr Biol* **10**, 1273-1282 (2000).
25. L. Blanchoin *et al.*, Direct observation of dendritic actin filament networks nucleated by Arp2/3 complex and WASP/Scar proteins. *Nature* **404**, 1007-1011 (2000).
26. A. Mogilner, G. Oster, Force generation by actin polymerization II: the elastic ratchet and tethered filaments. *Biophys J* **84**, 1591-1605 (2003).
27. M. Razbin, M. Falcke, P. Benetatos, A. Zippelius, Mechanical properties of branched actin filaments. *Phys Biol* **12**, 046007 (2015).
28. H. Kang, M. J. Bradley, W. A. Elam, E. M. De La Cruz, Regulation of actin by ion-linked equilibria. *Biophys J* **105**, 2621-2628 (2013).
29. B. L. Goode, M. O. Sweeney, J. A. Eskin, GMF as an Actin Network Remodeling Factor. *Trends Cell Biol* **28**, 749-760 (2018).
30. P. Bieling *et al.*, Force Feedback Controls Motor Activity and Mechanical Properties of Self-Assembling Branched Actin Networks. *Cell* **164**, 115-127 (2016).
31. V. I. Risca *et al.*, Actin filament curvature biases branching direction. *Proc Natl Acad Sci U S A* **109**, 2913-2918 (2012).
32. J. Mueller *et al.*, Load Adaptation of Lamellipodial Actin Networks. *Cell* **171**, 188-200 e116 (2017).
33. K. Hayakawa, H. Tatsumi, M. Sokabe, Actin filaments function as a tension sensor by tension-dependent binding of cofilin to the filament. *J Cell Biol* **195**, 721-727 (2011).
34. T. D. Pollard, J. A. Cooper, Actin, a central player in cell shape and movement. *Science* **326**, 1208-1212 (2009).
35. E. Ingerman, J. Y. Hsiao, R. D. Mullins, Arp2/3 complex ATP hydrolysis promotes lamellipodial actin network disassembly but is dispensable for assembly. *J Cell Biol* **200**, 619-633 (2013).
36. D. A. Fletcher, R. D. Mullins, Cell mechanics and the cytoskeleton. *Nature* **463**, 485-492 (2010).
37. L. Blanchoin, R. Boujemaa-Paterski, C. Sykes, J. Plastino, Actin dynamics, architecture, and mechanics in cell motility. *Physiol Rev* **94**, 235-263 (2014).
38. S. H. Parekh, O. Chaudhuri, J. A. Theriot, D. A. Fletcher, Loading history determines the velocity of actin-network growth. *Nat Cell Biol* **7**, 1219-1223 (2005).
39. R. E. Mahaffy, T. D. Pollard, Kinetics of the formation and dissociation of actin filament branches mediated by Arp2/3 complex. *Biophys J* **91**, 3519-3528 (2006).
40. R. E. Mahaffy, T. D. Pollard, Influence of phalloidin on the formation of actin filament branches by Arp2/3 complex. *Biochemistry* **47**, 6460-6467 (2008).
41. J. Berro, V. Sirotkin, T. D. Pollard, Mathematical modeling of endocytic actin patch kinetics in fission yeast: disassembly requires release of actin filament fragments. *Mol Biol Cell* **21**, 2905-2915 (2010).

42. V. Sirotkin, J. Berro, K. Macmillan, L. Zhao, T. D. Pollard, Quantitative analysis of the mechanism of endocytic actin patch assembly and disassembly in fission yeast. *Mol Biol Cell* **21**, 2894-2904 (2010).
43. M. Gandhi *et al.*, GMF is a cofilin homolog that binds Arp2/3 complex to stimulate filament debranching and inhibit actin nucleation. *Curr Biol* **20**, 861-867 (2010).
44. C. A. Ydenberg *et al.*, GMF severs actin-Arp2/3 complex branch junctions by a cofilin-like mechanism. *Curr Biol* **23**, 1037-1045 (2013).
45. H. Kang *et al.*, Site-specific cation release drives actin filament severing by vertebrate cofilin. *Proc Natl Acad Sci U S A* **111**, 17821-17826 (2014).
46. C. Chan, C. C. Beltzner, T. D. Pollard, Cofilin dissociates Arp2/3 complex and branches from actin filaments. *Curr Biol* **19**, 537-545 (2009).
47. G. I. Bell, Models for the specific adhesion of cells to cells. *Science* **200**, 618-627 (1978).
48. S. Rakshit, S. Sivasankar, Biomechanics of cell adhesion: how force regulates the lifetime of adhesive bonds at the single molecule level. *Phys Chem Chem Phys* **16**, 2211-2223 (2014).
49. A. Muhlrad, P. Cheung, B. C. Phan, C. Miller, E. Reisler, Dynamic Properties of Actin - Structural-Changes Induced by Beryllium Fluoride. *Journal of Biological Chemistry* **269**, 11852-11858 (1994).
50. P. Ge, Z. A. O. Durer, D. Kudryashov, Z. H. Zhou, E. Reisler, Cryo-EM reveals different coronin binding modes for ADP- and ADP-BeFx actin filaments. *Nature Structural & Molecular Biology* **21**, 1075-1081 (2014).
51. M. F. Carlier, D. Pantaloni, Binding of Phosphate to F-Adp-Actin and Role of F-Adp-Pi-Actin in Atp-Actin Polymerization. *Journal of Biological Chemistry* **263**, 817-825 (1988).
52. J. P. Robblee, W. Cao, A. Henn, D. E. Hannemann, E. M. De La Cruz, Thermodynamics of nucleotide binding to actomyosin V and VI: a positive heat capacity change accompanies strong ADP binding. *Biochemistry* **44**, 10238-10249 (2005).
53. E. W. Taylor, Kinetic studies on the association and dissociation of myosin subfragment 1 and actin. *J Biol Chem* **266**, 294-302 (1991).
54. J. A. Cooper, S. B. Walker, T. D. Pollard, Pyrene actin: documentation of the validity of a sensitive assay for actin polymerization. *J Muscle Res Cell Motil* **4**, 253-262 (1983).
55. L. A. Helgeson, B. J. Nolen, Mechanism of synergistic activation of Arp2/3 complex by cortactin and N-WASP. *Elife* **2** (2013).
56. A. C. Reymann *et al.*, Actin network architecture can determine myosin motor activity. *Science* **336**, 1310-1314 (2012).
57. Sonal *et al.*, Myosin-II activity generates a dynamic steady state with continuous actin turnover in a minimal actin cortex. *J Cell Sci* **132** (2018).
58. C. A. Wilson *et al.*, Myosin II contributes to cell-scale actin network treadmilling through network disassembly. *Nature* **465**, 373-377 (2010).
59. N. A. Medeiros, D. T. Burnette, P. Forscher, Myosin II functions in actin-bundle turnover in neuronal growth cones. *Nat Cell Biol* **8**, 215-226 (2006).
60. M. Vinzenz *et al.*, Actin branching in the initiation and maintenance of lamellipodia. *J Cell Sci* **125**, 2775-2785 (2012).
61. L. M. McMillen, D. Vavylonis, Model of turnover kinetics in the lamellipodium: implications of slow- and fast- diffusing capping protein and Arp2/3 complex. *Phys Biol* **13**, 066009 (2016).
62. T. Miyoshi *et al.*, Actin turnover-dependent fast dissociation of capping protein in the dendritic nucleation actin network: evidence of frequent filament severing. *J Cell Biol* **175**, 947-955 (2006).

63. D. E. Hannemann, W. X. Cao, A. O. Olivares, J. P. Robblee, E. M. De La Cruz, Magnesium, ADP, and actin binding linkage of myosin V: Evidence for multiple myosin V-ADP and actomyosin V-ADP states. *Biochemistry* **44**, 8826-8840 (2005).
64. E. V. Wong *et al.*, Nup159 Weakens Gle1 Binding to Dbp5 But Does Not Accelerate ADP Release. *J Mol Biol* **430**, 2080-2095 (2018).
65. M. Boczkowska, G. Rebowski, R. Dominguez, Glia Maturation Factor (GMF) Interacts with Arp2/3 Complex in a Nucleotide State-dependent Manner. *Journal of Biological Chemistry* **288**, 25683-25688 (2013).
66. K. Nakano, I. Mabuchi, Actin-depolymerizing protein Adf1 is required for formation and maintenance of the contractile ring during cytokinesis in fission yeast. *Mol Biol Cell* **17**, 1933-1945 (2006).
67. I. Rouiller *et al.*, The structural basis of actin filament branching by the Arp2/3 complex. *Journal of Cell Biology* **180**, 887-895 (2008).
68. B. R. McCullough, L. Blanchoin, J. L. Martiel, E. M. De la Cruz, Cofilin increases the bending flexibility of actin filaments: implications for severing and cell mechanics. *J Mol Biol* **381**, 550-558 (2008).
69. W. A. Elam *et al.*, Phosphomimetic S3D cofilin binds but only weakly severs actin filaments. *J Biol Chem* **292**, 19565-19579 (2017).
70. B. J. Nolen, T. D. Pollard, Structure and biochemical properties of fission yeast Arp2/3 complex lacking the Arp2 subunit. *J Biol Chem* **283**, 26490-26498 (2008).
71. B. Y. Hua *et al.*, An improved surface passivation method for single-molecule studies. *Nature Methods* **11**, 1233-+ (2014).
72. E. M. Johnson-Chavarria, U. Agrawal, M. Tanyeri, T. E. Kuhlman, C. M. Schroeder, Automated single cell microbioreactor for monitoring intracellular dynamics and cell growth in free solution. *Lab Chip* **14**, 2688-2697 (2014).
73. N. Courtemanche, J. Y. Lee, T. D. Pollard, E. C. Greene, Tension modulates actin filament polymerization mediated by formin and profilin. *Proc Natl Acad Sci U S A* **110**, 9752-9757 (2013).
74. C. Brennen, H. Winet, Fluid-Mechanics of Propulsion by Cilia and Flagella. *Annu Rev Fluid Mech* **9**, 339-398 (1977).
75. H. Kang *et al.*, Identification of cation-binding sites on actin that drive polymerization and modulate bending stiffness. *Proc Natl Acad Sci U S A* **109**, 16923-16927 (2012).
76. G. S. Manning, The molecular theory of polyelectrolyte solutions with applications to the electrostatic properties of polynucleotides. *Q Rev Biophys* **11**, 179-246 (1978).
77. T. Pujol, O. du Roure, M. Fermigier, J. Heuvingh, Impact of branching on the elasticity of actin networks. *Proc Natl Acad Sci U S A* **109**, 10364-10369 (2012).